Radium Isotopes Across the Arctic Ocean Show Time Scales of Water Mass Ventilation and Increasing Shelf Inputs

Author(s):
Rutgers van der Loeff, Michiel; Kipp, Lauren; Charette, Matthew A.; Moore, Willard S.; Black, Erin; Stimac, Ingrid; Charkin, Alexander; Bauch, Dorothea; Valk, Ole; Karcher, Michael; Krumpen, Thomas; Casacuberta, Núria; Smethie, William; Rember, Robert

Publication date:
2018-07

Permanent link:
https://doi.org/10.3929/ethz-b-000284551

Originally published in:
Journal of Geophysical Research: Oceans 123(7), https://doi.org/10.1029/2018JC013888

Journal of Geophysical Research: Oceans

RESEARCH ARTICLE
10.1029/2018JC013888

Radium Isotopes Across the Arctic Ocean Show Time Scales of Water Mass Ventilation and Increasing Shelf Inputs

Michiel Rutgers van der Loeff[1], Lauren Kipp[2], Matthew A. Charette[2], Willard S. Moore[3], Erin Black[2], Ingrid Stimac[1], Alexander Charkin[4], Dorothea Bauch[5], Ole Valk[1], Michael Karcher[1], Thomas Krumpen[1], Núria Casacuberta[6,7], William Smethie[8], and Robert Rember[9]

[1]Helmholtz Centre for Polar and Marine Research, Alfred Wegener Institute, Bremerhaven, Germany, [2]Department of Marine Chemistry and Geochemistry, Woods Hole Oceanographic Institution, Woods Hole, MA, USA, [3]Department of Earth and Ocean Sciences, University of South Carolina, Columbia, SC, USA, [4]Far Eastern Branch of Russian Academy of Sciences Russian Academy of Sciences (FEBRAS), Pacific Oceanological Institute (POI), Vladivostok, Russia, [5]GEOMAR Helmholtz Centre for Ocean Research Kiel, Kiel, Germany, [6]Laboratory of Ion Beam Physics, ETH Zurich, Zürich, Switzerland, [7]Environmental Physics, Institute of Biogeochemistry and Pollutant Dynamics, ETH Zürich, Zürich, Switzerland, [8]Lamont-Doherty Earth Observatory of Columbia University, New York, NY, USA, [9]International Arctic Research Center, University of Alaska Fairbanks, Fairbanks, AK, USA

Abstract The first full transarctic section of ^{228}Ra in surface waters measured during GEOTRACES cruises PS94 and HLY1502 (2015) shows a consistent distribution with maximum activities in the transpolar drift. Activities in the central Arctic have increased from 2007 through 2011 to 2015. The increased ^{228}Ra input is attributed to stronger wave action on shelves resulting from a longer ice-free season. A concomitant decrease in the ^{228}Th/^{228}Ra ratio likely results from more rapid transit of surface waters depleted in ^{228}Th by scavenging over the shelf. The ^{228}Ra activities observed in intermediate waters (<1,500 m) in the Amundsen Basin are explained by ventilation with shelf water on a time scale of about 15–18 years, in good agreement with estimates based on SF_6 and ^{129}I/^{236}U. The ^{228}Th excess below the mixed layer up to 1,500 m depth can complement ^{234}Th and ^{210}Po as tracers of export production, after correction for the inherent excess resulting from the similarity of ^{228}Ra and ^{228}Th decay times. We show with a Th/Ra profile model that the ^{228}Th/^{228}Ra ratio below 1,500 m is inappropriate for this purpose because it is a delicate balance between horizontal supply of ^{228}Ra and vertical flux of particulate ^{228}Th. The accumulation of ^{226}Ra in the deep Makarov Basin is not associated with an accumulation of Ba and can therefore be attributed to supply from decay of ^{230}Th in the bottom sediment. We estimate a ventilation time of 480 years for the deep Makarov-Canada Basin, in good agreement with previous estimates using other tracers.

Key Points:
- The increase of ^{228}Ra in central Arctic surface waters points at stronger sediment water exchange due to the longer ice-free season on Arctic shelves
- The decrease in ^{228}Th/^{228}Ra in the Transpolar Drift may be related to the increase in the rate of the drift
- Excess ^{228}Th in intermediate depths (100–1,500 m) may be used as tracer of export production

Supporting Information:
- Supporting Information S1
- Table S1
- Table S2
- Table S3a
- Table S3b
- Table S3c
- Table S4

Correspondence to:
M. Rutgers van der Loeff,
mloeff@awi.de

Citation:
Rutgers van der Loeff, M., Kipp, L., Charette, M. A., Moore, W. S., Black, E., Stimac, I., et al. (2018). Radium isotopes across the Arctic Ocean show time scales of water mass ventilation and increasing shelf inputs. *Journal of Geophysical Research: Oceans*, *123*, 4853–4873. https://doi.org/10.1029/2018JC013888

Received 12 FEB 2018
Accepted 21 MAY 2018
Accepted article online 31 MAY 2018
Published online 13 JUL 2018

1. Introduction

The Arctic Ocean is characterized by strong interactions with the surrounding continents. Over 10% of the world's river discharge finds its way into the Arctic Ocean, which has only 1% of the World's Ocean volume (McClelland et al., 2012). On the Siberian side, the shelves are especially wide and shallow. Surface waters in the central Arctic are relatively fresh, with the transpolar drift (TPD) serving as a transport route for terrestrial inputs through the central Arctic Ocean toward Fram Strait.

The Arctic Ocean is in transition. Minimum summer sea ice cover declined from 7 to 4 10^6 km^2 during the past 30 years (Grosfeld et al., 2016; Serreze et al., 2007). The longer ice-free period on the shelf and increased temperatures cause permafrost thaw (Luo et al., 2016) and increased erosion (Günther et al., 2013), which will affect the transport and fate of the terrestrial inputs. While these processes may enhance the input of sediments and dissolved material, the extensive sea ice melt may cause ice rafted matter to be released and deposited at an earlier stage on its transit over the Arctic Basins. The loss of sea ice will result in light conditions that are more favorable for plankton growth (Arrigo et al., 2008; Arrigo et al., 2012), but it is questionable whether there are sufficient nutrients for an increase in export production. It is therefore important to investigate whether the transport of terrestrial material, primary production, and sedimentation are affected in response to the environmental changes taking place.

Radium isotopes are particularly suited to study the transport and fate of terrestrial inputs in the Arctic. All four naturally occurring isotopes are produced by decay of an isotope of thorium, a highly particle reactive

element. Radium is relatively soluble in seawater such that once a thorium isotope in suspended or bottom sediments decays, a fraction of the produced radium isotope may be released to solution. ^{224}Ra (3.7-day half-life) and ^{223}Ra (11.4-day half-life) are used extensively as tracers for interaction on the shelf and for submarine groundwater discharge (SGD). ^{228}Ra is strongly enriched in shelf waters and in the TPD and its half-life (5.8 years) is well suited to study the fate of this shelf-derived water in the central Arctic (Rutgers van der Loeff et al., 1995). Finally, ^{226}Ra (1620 y half-life) has been used to trace SGD (Moore, 1996) and inputs from deep-sea sediments (Cochran, 1980).

Primary production and the export flux of particles are very low in the ice-covered Arctic Ocean. Cai et al. (2010) reported an export production of 0.2 ± 1.0 mmol carbon m^{-2} d^{-1} in the central Arctic Ocean based on ^{234}Th/^{238}U disequilibria measured in August to September 2007, but observations at the seafloor in 2012 suggested a more substantial export, for example, of ice algae (Boetius et al., 2013). One reason for this discrepancy may be that the time scale of the ^{234}Th tracer (related to the mean life of $1/\lambda$ = 35 days) is too short to record export events that took place earlier in the season. The time scale of the ^{210}Po/^{210}Pb tracer system (mean life of ^{210}Po is 200 days) is more appropriate to cover the full productive season. Roca-Martí et al. (2016) compared export fluxes using both tracer pairs. They confirmed low export fluxes in the central Arctic (2 ± 2 mmol C m^{-2} d^{-1} using ^{234}Th/^{238}U and 3 ± 2 mmol C m^{-2} d^{-1} using ^{210}Po/^{210}Pb) and observed a depletion of ^{210}Po at all stations, while a significant depletion of ^{234}Th was found in only three out of nine stations. Still, the calculated fluxes are low and have large uncertainties, and moreover, the use of ^{210}Po/^{210}Pb as tracer for export production is complicated by the particle reactive behavior of ^{210}Pb, which is itself scavenged. An alternative tracer pair with much promise for understanding Ocean export production is ^{228}Th/^{228}Ra (Luo et al., 1995; Rutgers van der Loeff et al., 2012). In the Arctic Ocean, activities of ^{228}Ra in surface waters are very high, the time scale of ^{228}Th can cover more than a productive season (^{228}Th half-life 1.9 years corresponding to a mean life of 2.7 years), and even the low export fluxes create a depletion that can be measured with good precision. A complicating factor of the relatively long time scale is that the ^{228}Th/^{228}Ra ratio in surface waters depends not only on the export flux but also on the scavenging history of the water mass (Rutgers van der Loeff et al., 2012). Here we wish to investigate to what extent the ^{228}Th/^{228}Ra ratio in the subsurface water column can be used to trace particle fluxes.

In this paper we present the distribution of ^{224}Ra, ^{228}Th, and ^{228}Ra in the surface water on a section from the Barents shelf to the Bering Strait, the first full transarctic section of these parameters measured as part of the coordinated GEOTRACES Arctic study in 2015. We compare the data with earlier observations and discuss the observed changes. The observed distributions of ^{228}Th and ^{228}Ra in the water column are compared with a Th/Ra profile model, and we discuss what these profiles can tell us about particle fluxes. Finally, we discuss to what extent the accumulation of ^{226}Ra that we observed in deep waters can be used as a measure of basin ventilation times.

2. Materials and Methods

In the framework of the GEOTRACES program, two expeditions were organized to the central Arctic in 2015: GEOTRACES section GN04 on RV *Polarstern* (expedition PS94, ARK XXIX/3, TRANSARC II; Schauer, 2016) and GEOTRACES section GN01 on USCGC Healy (expedition HLY1502; Kadko & Landing, 2015; Figure 1). We also report on Ra and Th analyses in surface waters collected on RV *Polarstern* expedition PS78/ARK XXVI/3 in 2011 (TRANSARC I) (Schauer, 2012). All data are presented in Tables S1–S4 in the supporting information.

During *Polarstern* expedition PS78 (5 August to 6 October 2011) large volume surface water samples were collected at 41 stations into 300-L tanks using a tap close to the ships seawater intake (first stations only) or (from North Pole Sta 218 onward) a well pump lowered over the side of the ship to a depth of 10 m. Each sample was filtered through a 0.8-μm Supor® (polyether sulfone) filter and then passed at a flow rate of <1 L/min using a peristaltic pump through MnO_2-impregnated acrylic fiber to scavenge radium isotopes. Fibers were partially dried using compressed air, and ^{224}Ra was measured at sea using RaDeCC delayed coincidence alpha detectors (Moore & Arnold, 1996). ^{224}Ra supported by ^{228}Th was derived from a second RaDeCC count after at least 20 days (5 half-lives).

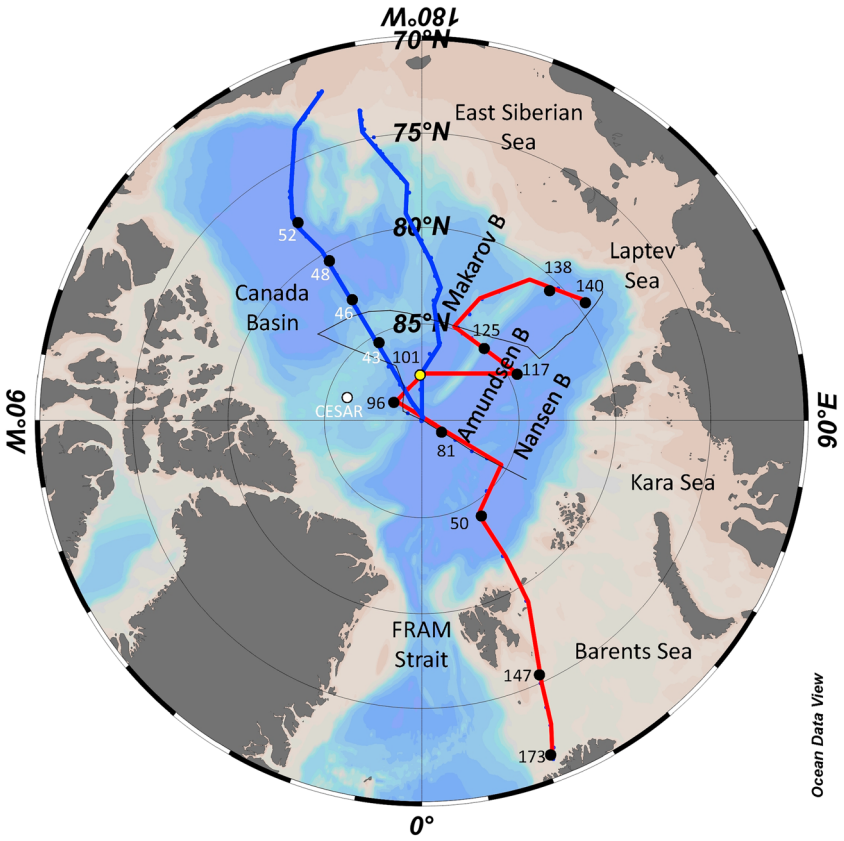

Figure 1. Cruise tracks of RV *Polarstern* expeditions PS78 (black), PS94 (GEOTRACES GN04, red, black station numbers), and USCGC Healy expedition HLY1502 (GEOTRACES GN01, blue, white station numbers) crossover station (yellow) and CESAR ice station (white dot).

During *Polarstern* expedition PS94 (17 August to 15 October 2015) surface water samples (collected at a tap close to the ships seawater intake after abundant rinsing of the tubing systems) were passed over an uncoated 7.5-cm cartridge and subsequently over a series of two tubes with loose MnO_2-coated fibers (up to Sta 96) or two MnO_2-coated cartridges (from Sta 99 onward; Henderson et al., 2013). Flow rate was limited to 1 L/min, and volumes were measured with Kent flow meters. During 10 in situ pump (ISP) casts, MnO_2-coated cartridges were mounted after 0.8-μm Supor filters; average flow rates varied between 0.8 and 6.1 L/min. On 37 ISPs two cartridges were used in series, allowing the calculation of Ra absorption efficiency. There was no relationship between Ra collection efficiency and flow rate ($R^2 = 0.0013$). On other ISPs only one cartridge could be mounted, in which cases we had to use the average collection efficiency of all other cartridges (90 ± 7%). Cartridges and fibers were partially dried using compressed air, and ^{224}Ra was measured at sea using RaDeCC delayed coincidence alpha detectors. Supported ^{224}Ra was derived from a second RaDeCC count after at least 16 days (4 half-lives).

Samples from PS78 and PS94 were analyzed for ^{226}Ra and ^{228}Ra at AWI, Bremerhaven. The fibers were leached following Elsinger et al. (1982), and the MnO_2-coated cartridges were leached by Soxhlet extraction with 6 N HCl refluxing over 10 hr. Radium in the extracts was coprecipitated with $BaSO_4$ (Cutter et al., 2010) and analyzed with gamma spectroscopy (Moore, 1984).

On the HLY1502 expedition, near-surface water samples were collected from a depth of 2 m using a submersible surface pump. Approximately 280 L of water was collected at each station and filtered through a MnO_2-coated fiber at a flow rate of <1 L/min. Over the shelf, the samples were first filtered through 1-μm Hytrex cartridge to remove particles; at all other stations, the samples were not prefiltered. The fibers were rinsed with Ra-free freshwater and analyzed on RaDeCC detectors within 3 days of collection to measure ^{224}Ra. After 4 weeks a second RaDeCC count was performed to determine the amount of ^{224}Ra supported by

^{228}Th. Fibers were then ashed in a muffle furnace at 820 °C, and the ash was packed in to polystyrene vials, sealed with epoxy (to prevent ^{222}Rn loss), aged for 3 weeks, and analyzed on high purity, well-type gamma detectors in the Moore lab at the University of South Carolina. Radium-228 was measured using the lines of ^{228}Ac (338 and 911 KeV), and ^{226}Ra was measured using the line for ^{214}Pb (352 KeV). Detector efficiencies were determined using ashed fiber standards spiked with ^{226}Ra and ^{232}Th with daughters in equilibrium.

Water column samples for the HLY1502 expedition were collected using ISPs that were programmed to pump for 4 hr, typically filtering 1,200–1,600 L of seawater at an average flow rate of ~6 L/min. Seawater was first passed through 51 and 1-μm filters to collect particulate isotopes, and then through MnO_2-coated cellulose cartridges (Henderson et al., 2013). After collection, cartridges were rinsed with Ra-free freshwater, partially dried with compressed air, and counted on RaDeCC detectors within 2 days of collection to measure ^{224}Ra. Second counts were performed after 4 weeks to determine the amount of supported ^{224}Ra. Cartridges were then ashed, and ^{228}Ra and ^{226}Ra were measured by gamma spectrometry in the Charette lab at the Woods Hole Oceanographic Institution using the same method as the surface samples. To determine cartridge collection efficiencies, small volume samples of ^{226}Ra (15–25 L) were collected using a Niskin bottle mounted either on the CTD rosette (shallow casts) or above the ISPs (deep casts) and were filtered through a MnO_2-coated fiber. The activities of Ra measured on the fibers, which quantitatively scavenge radium (Charette et al., 2012), were compared to those determined on the cartridges. For HLY1502, the collection efficiency of individual cartridges ranged from 19% to 99%, with an average of 70 ± 19% (1σ). Particulate ^{228}Th activities were measured on the 51 and 1-μm filters using RaDeCC detectors after storing the samples for at least a month to allow ^{224}Ra to reach secular equilibrium with ^{228}Th (Black, 2018; Maiti et al., 2014).

For the intercalibration of RaDeCC counting (^{224}Ra), cartridges spiked with ^{232}Th series in equilibrium were prepared in the USC lab of Willard Moore in South Carolina and in the AWI lab in Bremerhaven. These standards were circulated among the Charette, Moore, and Rutgers van der Loeff labs and results agreed to within 9–13%, comparable to interlab differences for high ^{224}Ra activities in a previous intercalibration (Charette et al., 2012). For the intercalibration of gamma counting (^{226}Ra and ^{228}Ra) a fiber spiked at the WHOI lab with the WHOI ^{226}Ra/^{228}Ra standard was analyzed at AWI. AWI values were 4.1 ± 1.7% lower for ^{226}Ra and 6.4 ± 2.2% higher for ^{228}Ra compared to the WHOI calibration. A further check was obtained from the sampling at the crossover station: Healy HLY1502 station 30 (1 September 2015) and *Polarstern* PS94 station 101 (14 September 2015; Figure S1 in the supporting information). The offset in ^{226}Ra likely results from the fact that the HLY1502 analyses were performed on discrete samples, whereas the PS94 analyses depended on the estimate of the cartridge collection efficiency. In this paper we only discuss ^{226}Ra data of the PS94 expedition.

3. Results

3.1. Surface Distribution ^{228}Ra

The surface distribution of ^{228}Ra (Tables S2 and S3 and Figure 2a) shows the prominent enrichment of this isotope in the TPD. Earlier studies had shown this enrichment (Rutgers van der Loeff et al., 1995; Rutgers van der Loeff et al., 2012; Smith et al., 2003), but this is the first full transarctic section showing in a synoptic study the extension of the ^{228}Ra plume with its limits in the Eurasian and the Canadian side of the TPD.

3.2. Surface Water ^{228}Th-^{224}Ra Systematics

From the two RaDeCC counts of uncoated and coated cartridges that had been collected in surface waters on the *Polarstern* expedition PS94, we calculated particulate and dissolved ^{224}Ra and ^{228}Th, decay/ingrowth corrected to sampling time (Table S2 and Figure 3). As expected, the particulate ^{224}Ra activity was negligible, but particulate ^{228}Th contributed up to 50% of total ^{228}Th.

Excess ^{224}Ra (^{224}Ra$_{xs}$) is defined as ^{224}Ra not supported by ^{228}Th. In order to take into account the particulate ^{228}Th activity, we distinguish between dissolved and total ^{224}Ra$_{xs}$:

$$\text{diss}^{224}\text{Ra}_{xs} = {}^{224}\text{Ra}_{diss} - {}^{228}\text{Th}_{diss} \quad (1)$$

$$\text{Total}^{224}\text{Ra}_{xs} = {}^{224}\text{Ra}_{diss} + {}^{224}\text{Ra}_{part} - {}^{228}\text{Th}_{diss} - {}^{228}\text{Th}_{part} \quad (2)$$

Usually, ^{224}Ra$_{part}$ is negligible (cf. Table S2) giving

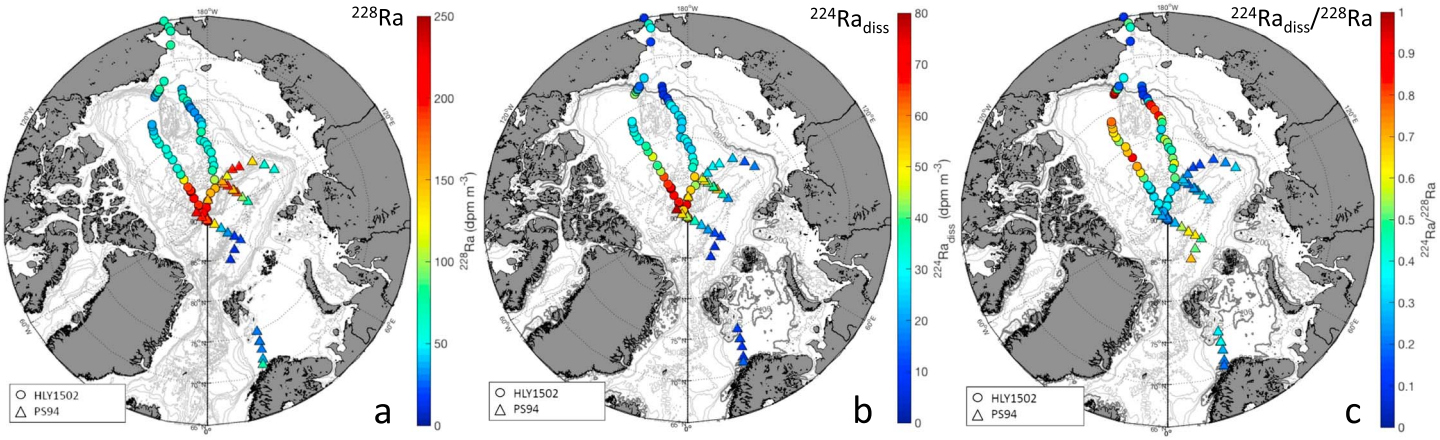

Figure 2. Distribution of (a) ^{228}Ra, (b) $^{224}Ra_{diss}$ as analogue for total ^{228}Th, and (c) $^{224}Ra_{diss}/^{228}Ra$ as analogue for total $^{228}Th/^{228}Ra$ ratio in surface waters in 2015.

$$\text{Total}^{224}Ra_{xs} = {}^{224}Ra_{diss} - {}^{228}Th_{diss} - {}^{228}Th_{part} \quad (3)$$

Most of the dissolved ^{224}Ra that was not supported by dissolved ^{228}Th (i.e., dissolved $^{224}Ra_{xs}$) was actually supported by particulate ^{228}Th (Figure 3). As expected from the shelf sources of ^{224}Ra, total $^{224}Ra_{xs}$ was a significant fraction of the total ^{224}Ra on the Barents shelf (stations PS94–147 to 161). Although in an exceptional case Kadko and Muench (2005) once observed some excess ^{224}Ra up to 200 km from the shelf source, we do not expect excess ^{224}Ra in the central Arctic Ocean. Indeed, in the central Arctic, total $^{224}Ra_{xs}$ is generally a small fraction of total ^{224}Ra (Figure 3). Nevertheless, at many stations from the TPD, we find significant fractions of total $^{224}Ra_{xs}$ reaching 40% of ^{224}Ra at station PS94–96 (Figure 3). We cannot completely exclude some ^{224}Ra release from ^{228}Th adsorbed to the tubing of the ship, although we have tried to minimize this problem (see methods). Such a contamination would be expected to aggravate during passage in high-^{228}Th waters. The observation that after passing the high-^{228}Th waters of the TPD the absolute levels of total $^{224}Ra_{xs}$ actually decreased (Figure 3: Stations 137, 138, and even the Barents Shelf stations 147–173) makes it unlikely that this contamination can explain the observed total $^{224}Ra_{xs}$. Such a contamination

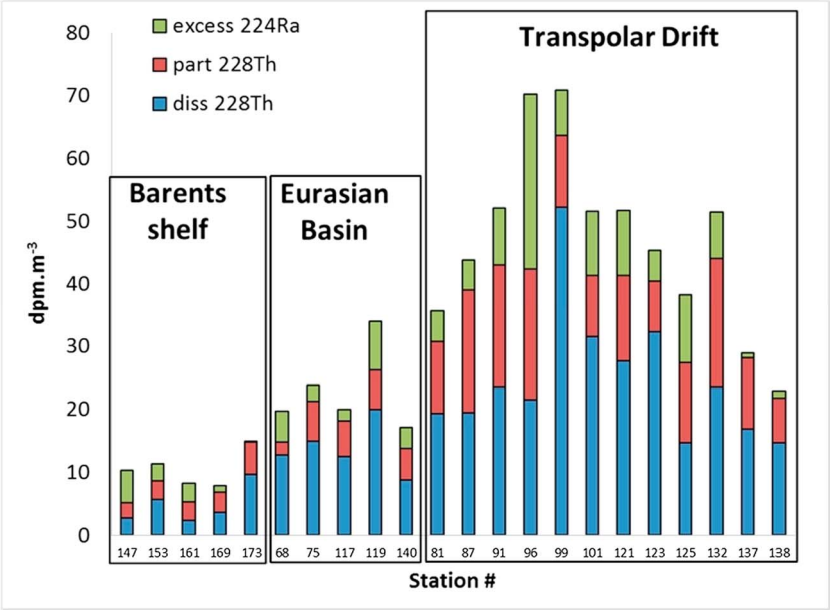

Figure 3. Dissolved (blue) and particulate (red) ^{228}Th and total excess ^{224}Ra activities (green) in surface waters of the PS94 expedition, grouped in the three regions Barents shelf, Eurasian Basin, and transpolar drift.

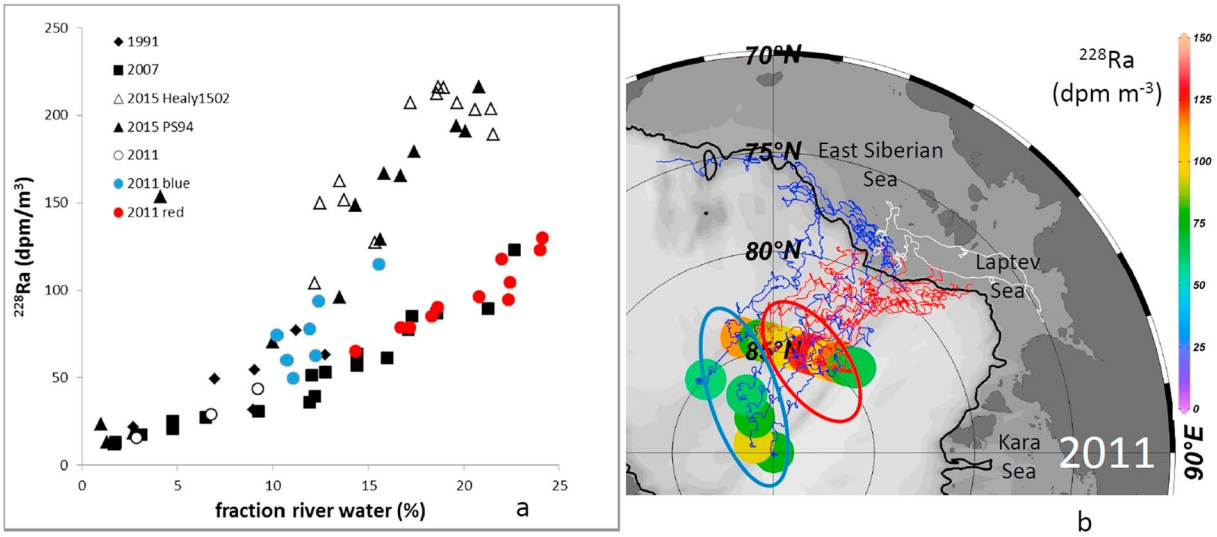

Figure 4. (a) ^{228}Ra as function of fraction meteoric water for surface water samples collected North of 84°N in 1991, 2007, 2011, and 2015, highlighting stations in 2011 (PS78) with high ^{228}Ra (>50 dpm m^{-3}) that populate two groups with distinct slopes. Stations within the blue oval (blue dots in (a)) have higher ^{228}Ra activities than stations within the red oval (red dots); (b) Ice back-trajectories (IBTs) of stations highlighted in panel a showing that the samples collected in 2011 with higher ^{228}Ra activities (blue symbols in (a), blue oval and IBTs) have their origin further east than the samples with lower activities (red symbols in (a), red oval and IBTs). IBTs extending more than 2 years before sampling (Sta 224 and 227 from blue region) shown in white and 250-m depth contour highlighted in black.

cannot occur in the ISPs casts deployed on the Healy from 20 m downward. Two of the 20-m samples, station HLY1502–38 (87°N) and station HLY1502–46 (82°N), had significant total ^{224}Ra$_{xs}$. The total ^{224}Ra$_{xs}$ observed in surface water at these latitudes may be due to ^{224}Ra released from ^{228}Th carried in ice-rafted particles.

3.3. Surface Distribution ^{228}Th and ^{228}Th/^{228}Ra

Because our study is concentrated on the shelf signals observed in the central Arctic far offshore, we disregard total ^{224}Ra$_{xs}$ and estimate total ^{228}Th from dissolved ^{224}Ra (equation (3)) which is available for all cruises reported here (Tables S1–S4). For PS94 we have independent data for dissolved and particulate ^{228}Th, but for a consistent comparison with the other expeditions, we choose to present the distribution of dissolved ^{224}Ra as an analogue for total ^{228}Th (Figure 2b), an approach that may have caused a 17% overestimation of ^{228}Th (Figure S2b). The ^{228}Th/^{228}Ra activity ratio, which is low (order of 0.1–0.2) on the shelf as a result of scavenging (Rutgers van der Loeff et al., 2012), remains fairly low (<0.4) in the core of the TPD (Figure 2c). Only in the central Eurasian and Canada Basins are higher activity ratios reached.

3.4. Changes With Time in Surface Water

3.4.1. ^{228}Ra

Kipp et al. (2018) observed that ^{228}Ra in the TPD had increased from 2007 to 2015. They plotted ^{228}Ra as a function of the fraction of meteoric water in order to show that the increase was not a result of a changed river water concentration that might have resulted from a change in freshwater accumulation in the Arctic (Rabe et al., 2014). Here we extend their plot with data from the *Polarstern* PS78 (2011) and PS94 (2015) expeditions (Figure 4a). The PS94 data from 2015 are in line with the parallel data collected on the Healy (Kipp et al., 2018), confirming the increase relative to 2007. The data from 2011 show two distinct trends: All samples collected on the detailed section over the Lomonosov Ridge closest to the Siberian shelf follow perfectly the mixing line we had observed in 2007. But the four samples with the highest ^{228}Ra concentrations on the Canadian side of the cruise track are close to the mixing line we observed throughout in 2015, suggesting the existence of two different freshwater end-members in 2011.

3.4.2. ^{228}Th/^{228}Ra

In surface waters, ^{228}Th was more depleted with respect to its parent ^{228}Ra in 2015 than it was in the previous expeditions in 2007 and 2011 (Figure 5). The decrease of ^{228}Th/^{228}Ra is especially pronounced in the TPD: The ^{228}Th/^{228}Ra in the shelf-influenced waters north of 85°N with river water percentage > 13% are consistently low at about 0.3 in both the *Polarstern* PS94 and the Healy data set, compared to 0.5–0.65 in 2007.

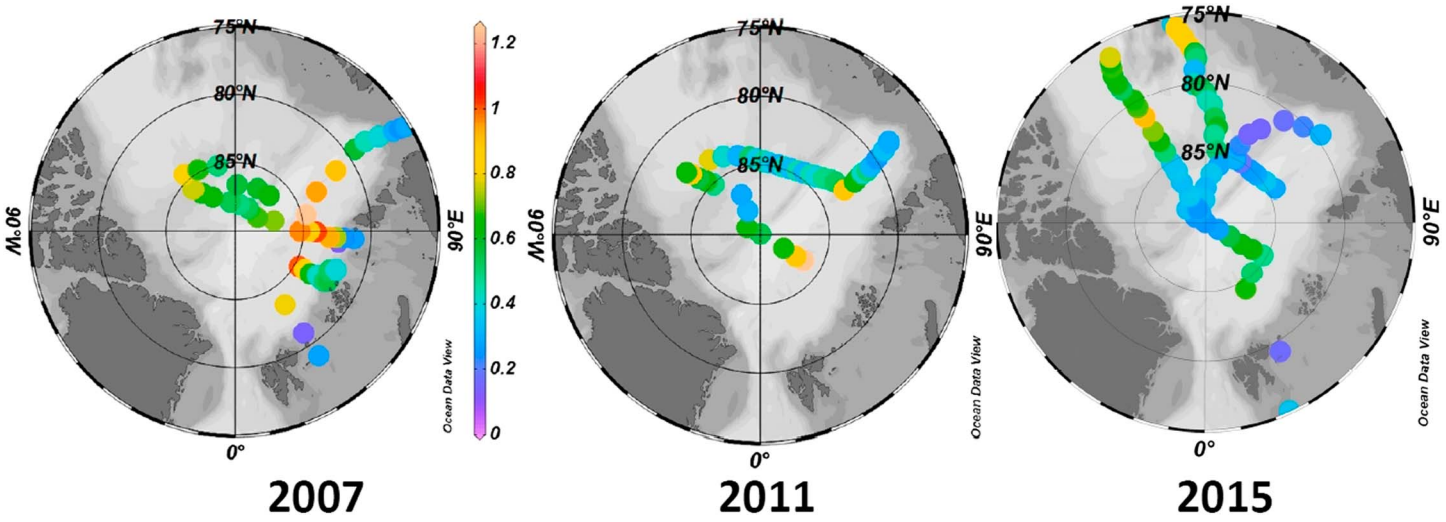

Figure 5. $^{224}Ra/^{228}Ra$ ratio as analogue for $^{228}Th/^{228}Ra$ ratio in surface waters in 2007, 2011, and 2015.

3.5. Distribution of ^{228}Ra and ^{228}Th in the Water Column

The distribution of ^{228}Ra in the water column of the Eurasian and Makarov Basins (Figure 6a) is in agreement with earlier observations (Cochran et al., 1995; Rutgers van der Loeff et al., 1995; Trimble et al., 2004). The high ^{228}Ra activities in the surface waters and especially in the TPD cause very strong gradients through the halocline. ^{228}Ra activities in deep water (2,000–3,000 m) are low but still measurable and slightly increase toward the bottom.

We estimate the depth profiles of ^{228}Th from measurements of $^{224}Ra_{diss}$ that we made at all stations. This implies that (1) we disregard excess ^{224}Ra as we did in the discussion of the surface concentrations (Figure 2b) and (2) we assume that total (dissolved + particulate) ^{228}Th is in secular equilibrium with dissolved ^{224}Ra. A comparison of dissolved ^{224}Ra with total (dissolved + small particulate + large particulate) ^{228}Th for the HLY1502 expedition confirms that ^{224}Ra is a reasonably good analogue for total ^{228}Th, although ^{224}Ra may underestimate total ^{228}Th by about 10% (Figure S2a).

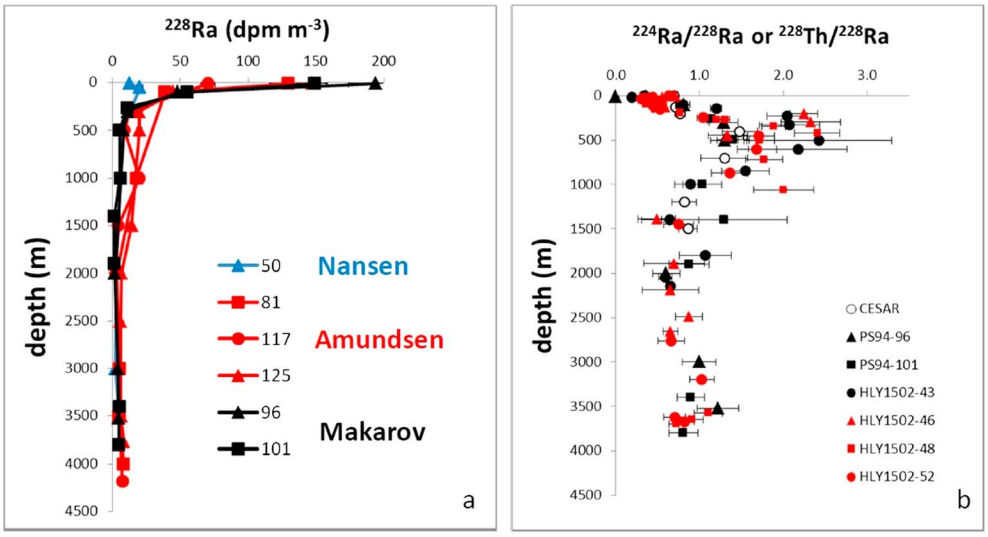

Figure 6. (a) Depth profiles of ^{228}Ra distinguishing PS94 stations from the Nansen (blue), Amundsen (red), and Makarov Basin (black) and (b) $^{224}Ra/^{228}Ra$ as analogue for $^{228}Th/^{228}Ra$ ratio observed in the Makarov (black) and Canada (red) basin compared with $^{228}Th/^{228}Ra$ data from ice station CESAR (Bacon et al., 1989).

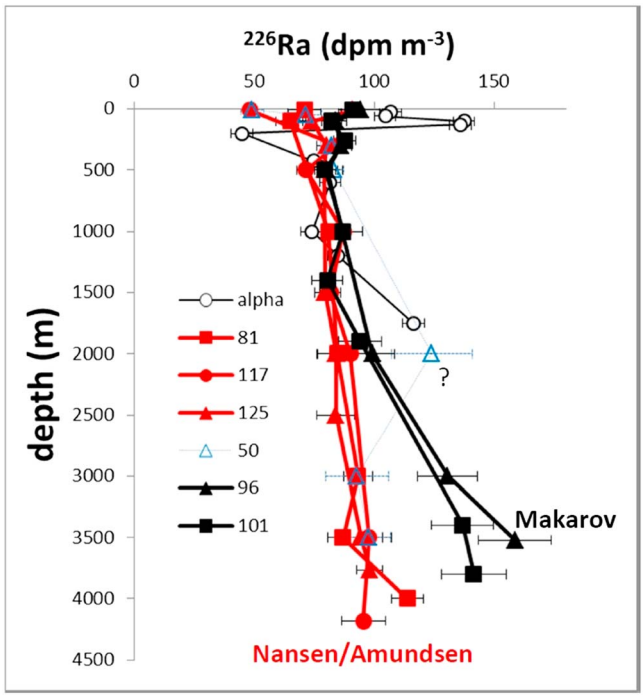

Figure 7. Depth profiles of ^{226}Ra distinguishing PS94 stations from the Nansen (open triangles), Amundsen (red), and Makarov Basin (black) compared to the profile measured in 1983 at CESAR ice station over the Alpha Ridge (open circles, Moore & Smith, 1986). We have no explanation for the high value at 2,000 m at Sta 50.

Two depth profiles of ^{228}Th have been reported for the Nansen Basin by Cochran et al. (1995): one from the Barents Slope (their Sta. 287) and one from the central Nansen Basin (their Sta. 358). ^{228}Th/^{228}Ra ratios reported by these authors approached unity at mid depth in the central Nansen Basin but remained below 0.6 at the slope station with an average of 0.42. The only two ^{228}Th/^{228}Ra profiles we are aware of from the deep Canada Basin are the CESAR Ice station (Bacon et al., 1989) and station AWS2000-3 (Trimble et al., 2004). While at AWS2000-3 (75°13′N, 3,850 m) ^{228}Th/^{228}Ra increased gradually to a value of 1.1 ± 0.4 at 2,000 m, the CESAR profile at the Alpha Ridge showed depletion around 0.75 in the upper 200 m, then a maximum of 1.48 ± 0.21 at 400 m and a decrease to values below unity at 1,200 and 1,500 m. Such a subsurface maximum was also observed in the Atlantic Ocean by Li et al. (1980). Our new data (Figure 6b, $^{224}Ra_{diss}$/^{228}Ra in Tables S1 and S3c) are in general agreement with the CESAR profile: They confirm the depleted ^{228}Th/^{228}Ra ratios in surface waters. Below the surface of the TPD both ^{228}Th and ^{228}Ra decline abruptly, but the ^{228}Th/^{228}Ra ratio increases to values usually in excess of unity in the 250–1,500 m depth range. In waters of 2,000 m and below, the ratio is usually below unity (0.75 ± 0.05 standard error of mean, n = 28).

3.6. ^{226}Ra

Previous studies of Ra in the deep Arctic Ocean have mostly reported ^{228}Ra/^{226}Ra ratios where ^{226}Ra was estimated from relationships with Si (Cochran et al., 1995; Rutgers van der Loeff et al., 1995). Moore and Smith (1986) reported a profile at station CESAR over the Alpha Ridge and observed that the deepest sample (1,750 m) was enriched in ^{226}Ra by 40 dpm m^{-3} relative to the samples at 500–1,000 m, much more than the about 3 dpm m^{-3} expected from the increase in silicate of only 3 μmol/kg. The depth distribution of ^{226}Ra on cruise PS94 confirms an enrichment of ^{226}Ra in deep waters (Figure 7). In the Nansen and Amundsen Basins the deep waters below approx. 2,000 m are enriched by about 10–15 dpm m^{-3}, whereas the deep waters in the Makarov Basin are enriched by up to 80 dpm m^{-3} relative to the average concentrations in intermediate waters of 500–1,500 m (Figure 7 and Table S1). Integrating these excess activities with depth we find an excess inventory of 20,000 dpm m^{-2} in the Nansen and Amundsen Basin and 70,000 dpm m^{-2} in the Makarov Basin.

4. Discussion

4.1. Reasons for Change in ^{228}Ra

Some ^{228}Ra is supplied by rivers, but the major source of ^{228}Ra in the Arctic is released from the seafloor where it is produced by decay of ^{232}Th. The accumulation of ^{228}Ra in shelf waters depends on the depth of the shelf sea and on the time the water resides over the shelf. The high ^{228}Ra activities in surface waters of the TPD have traditionally been explained by the wide extent of Siberian shelf seas with depths decreasing eastward from the Barents and Kara Sea toward the very shallow East Siberian Sea. The correlation of ^{228}Ra in offshore surface waters with salinity and with the fraction of meteoric water is due to the common nearshore source of ^{228}Ra and meteoric water. This results in a virtual freshwater end-member that is not actually observed in river waters (Rutgers van der Loeff et al., 2003).

Our results from *Polarstern* 2015 (PS94) confirm the conclusion of Kipp et al. (2018) that the ^{228}Ra concentration in the virtual freshwater end-member of the ^{228}Ra on the Siberian shelf has roughly doubled since 2007 (Figure 4a). If this change had occurred gradually, we would have expected the results for 2011 to be intermediate between 2007 and 2015. It is very surprising that they are not, but indeed follow the mixing lines of 2007 and 2015 in two discrete geographical regions represented in Figure 4b by red and blue ovals, respectively. Ice back-trajectories (IBTs; Krumpen, 2017) show that the ice found in these regions was formed in distinct shelf sources (Figure 4b). To the extent that ice follows surface water flow, this implies that the

surface water at the stations with high meteoric water content and a lower virtual freshwater end-member ^{228}Ra activity (indicated by red symbols in Figure 4a and by red ovals and red IBTs in Figure 4b) has a more westerly origin in the Laptev Sea region, whereas the high-^{228}Ra water at the stations in the blue oval comes from a source further east, influenced by the East Siberian Shelf. This demonstrates that we cannot assume that all ^{228}Ra values observed offshore in the Arctic Ocean have a similar virtual freshwater end-member. The ice at two stations in the blue oval (PS78–224 and 227) was more than 2 years old. The ice was formed in the Laptev Sea (white lines in Figure 4b) but then spent 15 months on the shelf north of the North Siberian Islands where the water can have accumulated additional ^{228}Ra before being carried northward. The existence in 2011 of two source regions with distinct virtual ^{228}Ra end-member activities raises the question whether the apparent differences in ^{228}Ra activities between 2007 and 2015 (Figure 4a) can also be due to sources with distinct end-member concentrations resulting from changes in flow paths and/or shelf residence times.

Some insight into the possible role of circulation changes in the interannual differences between ^{228}Ra at the surface can be gained from model experiments. We have used the coupled sea ice ocean model NAOSIM to disperse a conservative tracer released in Bering Strait (e.g., Aksenov et al., 2016) and the anthropogenic radionuclide ^{129}I, released from the European reprocessing facilities in La Hague and Sellafield (Karcher et al., 2012). While the former serves as a tracer for Pacific Water on its way across the Chukchi and East Siberian Seas, the latter, due to the dominant advection of the ^{129}I along the Siberian shelves from the Barents Sea via the Kara Sea into the Laptev Sea, can be used as an indicator for the pathway of Kara and Laptev Sea water into the central Arctic. Typically, the bulk of the waters in the Amerasian Basin stem from Pacific derived waters. The borderline between waters dominantly derived from the Pacific (via the East Siberian Sea) and the Atlantic (via the Kara and Laptev Sea), however, varies, due to changes of the surface circulation, for example, as a consequence of changing atmospheric conditions. Figure 8 shows the distribution of ^{129}I for September 2007, 2011, and 2015 in comparison with the distribution of ^{228}Ra in these years. The Pacific water tracer (not shown) gives a largely complementary picture, as expected. For 2007 the position of stations with elevated ^{228}Ra was over the Alpha Ridge and in the Makarov Basin close to the North Pole. The model simulation suggests that this is an area where the front between the water stemming from the East Siberian shelves and the Laptev/Kara Sea shelves was located in this period. Water from both source regions would be similarly likely to be found here. In 2011 the situation was different. For this year the model suggests, in agreement with the IBT analysis, that the stations closer to the New Siberian Islands (red oval in Figure 4b) are mostly derived from water stemming from the Laptev/Kara Sea. Only the stations closer to the North Pole (blue oval in Figure 4b) are likely to incorporate water stemming from the East Siberian Sea. For the year 2015 finally, the model simulation indicates a source region to be entirely from the Laptev/Kara Sea region for those stations with elevated ^{228}Ra found in the Makarov Basin.

Essential for the accumulation of ^{228}Ra is how long the water passed over shallow shelf areas. That is why we need actual flow paths that can be based on modeling (Figure 8) and on IBTs. Kipp et al. (2018) concluded from IBT analyses that the shelf origin of the high-^{228}Ra waters found in the central Arctic was not different for the stations visited in 2015 by USCGC Healy or those from the 2007 study. This is confirmed by an IBT analysis of the *Polarstern* 2015 (PS94) study (Figure S3a). The history of the water masses before the time span of the IBTs was nevertheless quite different, as the NAOSIM modeling (Figure 8) suggested that the 2007 samples were from both sides of the Atlantic-Pacific divide, whereas the 2015 samples had a large Atlantic component. We have seen in the 2011 data that different histories can cause different ^{228}Ra concentrations and a temporal increase in the residence time over a shelf could produce a water mass with high ^{228}Ra concentrations. It would be of great value to have data on the variability of residence times of water over the Siberian shelves. But the increase in ^{228}Ra concentrations in 2015 compared to earlier years is so widespread (Figure 8) that it is unlikely that it is caused by such a stagnation event and we conclude that indeed the input of ^{228}Ra has increased. There are several possible explanations for this increase (Kipp et al., 2018). SGD is in many ocean areas a major pathway for inputs of ^{228}Ra to the ocean (Moore et al., 2008). Due to the wide extent of permafrost it has been doubted whether SGD plays a role in the Arctic Ocean, but ^{228}Ra inputs from this source have been identified by a recent study in the Laptev Sea (Charkin et al., 2017). However, because of the ubiquitous presence of ^{238}U and ^{232}Th in soils, SGD supplies ^{226}Ra along with ^{228}Ra. If an increase in SGD had resulted from an increase in the flow of old groundwater or from the exposure of recently thawed subsea permafrost to seawater circulation, we would expect their ^{228}Ra/^{226}Ra ratios to be closer to the crustal ratio of ~1.

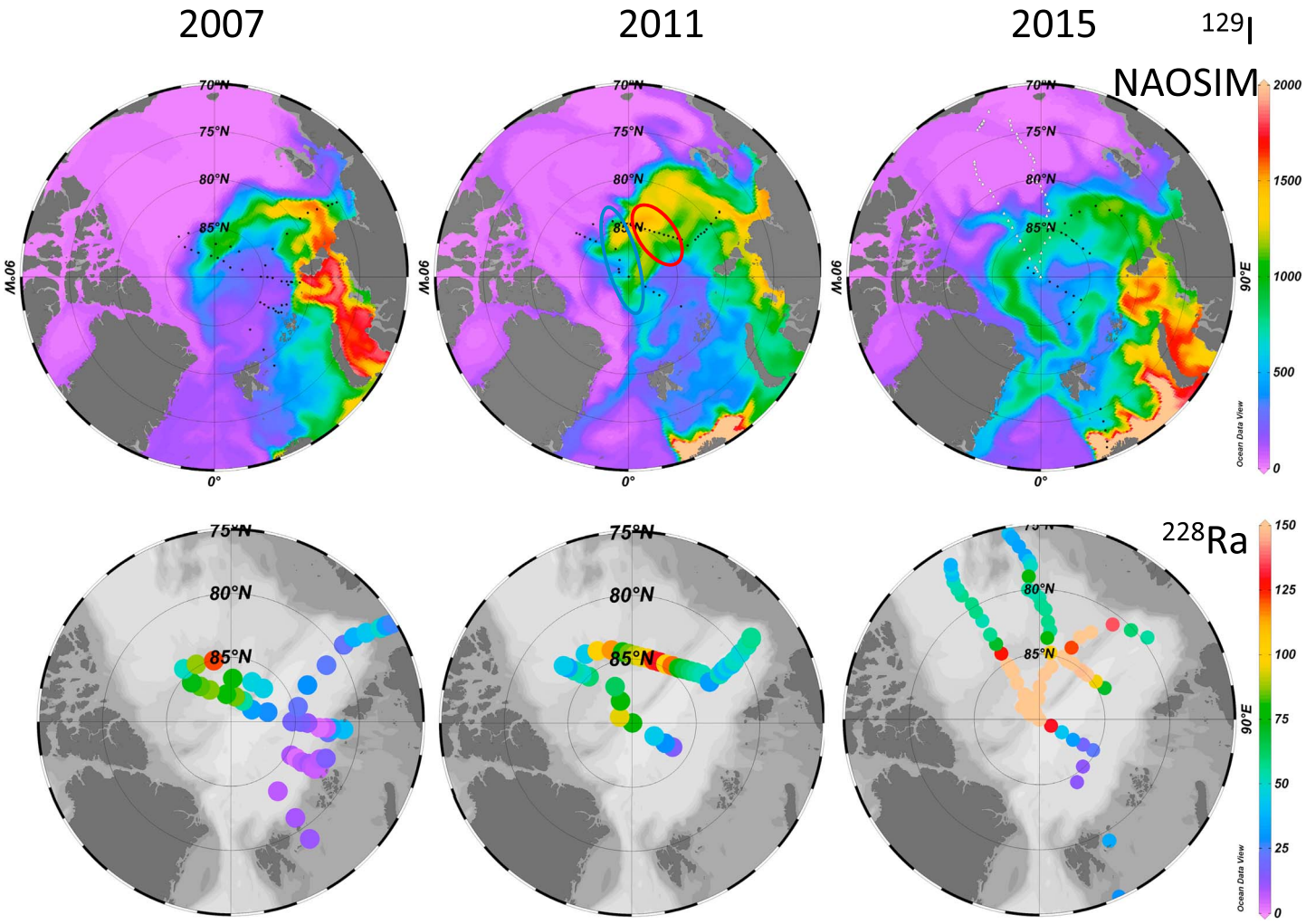

Figure 8. NAOSIM model simulation of the distribution of ^{129}I (10^7 at/L) for the Septembers in 2007, 2011, and 2015 in comparison with the distribution of ^{228}Ra (dpm m^{-3}) in these years. The blue and red ovals in the middle upper panel represent regions where ^{228}Ra and IBTs suggest that the surface water stems from the East Siberian and Kara/Laptev shelves, respectively (Figures 4a and 4b).

The relatively small enrichment of ^{226}Ra in the TPD (Kipp et al., 2018) is an indication that SGD is not a major contributor to the increase in ^{228}Ra.

Coastal erosion is increasing in the Arctic, enhanced by temperature rise and permafrost thaw. This will certainly contribute ^{228}Ra to coastal waters, but this source is insufficient to explain the increase of ^{228}Ra in the TPD (Kipp et al., 2018). Moreover, just like SGD, coastal erosion is a source of ^{226}Ra along with ^{228}Ra, and a parallel increase in ^{226}Ra is not observed.

The most likely explanation for the increase in ^{228}Ra is therefore increased resuspension and pore water exchange due to the enhanced exposure of shelf sediments to wave action. As a result of sea ice retreat, larger areas of the continental shelf are ice-free for a longer period of the year. And such a sediment source would supply relatively higher amounts of ^{228}Ra relative to ^{226}Ra due to the faster regeneration time of the former.

4.2. Changes in Other Terrigenous Inputs in the TPD

In the TPD, waters with a high meteoric contribution flow from the Siberian shelves toward Fram Strait. The extent of this ~50–100 m thick shelf-influenced layer is clearly seen in the surface distribution of ^{228}Ra (Figure 2a) but also is clearly visible in the distribution of various terrigenous components like Fe, Mn, and

DOM (Klunder et al., 2012; Middag et al., 2011; Slagter et al., 2017). Middag et al. (2011) and Klunder et al. (2012) argue that rivers are the main source of Mn and Fe to the TPD. Along with these trace metals, the TPD also transports ligands and other DOM.

Just like ^{228}Ra (Figure 4a), other terrigenous components like dissolved Fe (Klunder et al., 2012; Slagter et al., 2017) and DOM (Stedmon et al., 2011) are correlated with the fraction of meteoric water, while Fe and iron-binding organic ligands are correlated with CDOM and humic substances (Slagter et al., 2017). This raises the question of whether the increase in ^{228}Ra is accompanied by a similar increase in these other terrigenous constituents. In contrast to ^{228}Ra, where shelf inputs are predominant and we defined a virtual freshwater end-member, DOM and other terrigenous components like REE (Laukert et al., 2017) have primarily freshwater sources. The correlation between ^{228}Ra and such river borne terrigenous components (not shown) is therefore in part fortuitous because the sources of these terrigenous inputs do not coincide. Inputs of Fe, Fe ligands, Mn, and CDOM to the TPD will only increase along with ^{228}Ra to the extent that their sources are on shelf sediments, not in the rivers.

4.3. Reasons for Change in ^{228}Th/^{228}Ra

The development of ^{228}Th/^{228}Ra in the TPD with time t since the water mass lost contact with the shelf follows (Rutgers van der Loeff et al., 2012, note typo corrected here)

$$A_T = A_{T^0} e^{-(\lambda_T+\lambda_s)t} + \frac{\lambda_T}{\lambda_T+\lambda_s-\lambda_R} A_{R^0}\left(e^{-\lambda_R t} - e^{-(\lambda_T+\lambda_s)t}\right) \quad (4)$$

where A_T and A_R are the activities of ^{228}Th and ^{228}Ra, λ_T and λ_R the decay constants of ^{228}Th and ^{228}Ra, respectively, λ_s is the Th scavenging rate, and superscript ^{0} denotes the situation at $t = 0$ when the water leaves the shelf. In equation (4) we assume that lateral mixing is unimportant relative to advection in the TPD. In our 2007 study we found that ^{228}Th/^{228}Ra was about 0.15 on the shelf and increased to 0.4–0.6 in the TPD in the central Arctic. In 2011, ^{228}Th/^{228}Ra in samples in the TPD ($f_r > 15\%$) ranged from 0.31 to 0.49, while in 2015, the ^{228}Th/^{228}Ra values were significantly lower (0.2–0.35) than in 2007. In all these surface water data the use of dissolved ^{224}Ra as analogue for total ^{228}Th may have caused an overestimation of ^{228}Th (Figure S2b), but the procedure was the same in all three expeditions and cannot have caused the observed trend. The decrease could be due to one or a combination of several reasons:

Recent increase in ^{228}Ra: equation (4) assumes a constant source concentration of ^{228}Ra while we have found an increase over the past 8 years. The ingrowth of ^{228}Th will lag behind. However, because the time change (8 years) is slow relative to the half-life of ^{228}Th, we disregard this lag effect.

Lower depletion on the shelf: In 2015 we have few data of ^{228}Th$_{part\ +\ diss}$/^{228}Ra from the eastern Arctic shelves. On the Barents shelf we found 0.18–0.19, and the lowest values on the approach of the Laptev shelf were 0.14–0.16. We assume that ^{228}Th/^{228}Ra has remained depleted to about 0.15 before leaving the shelf.

A higher scavenging rate (lower λ_s) would counteract the ingrowth and explain lower ^{228}Th/^{228}Ra values. If sufficient nutrients are available, the reduction in ice cover could cause increased productivity (Arrigo et al., 2008) and consequently increased export flux and scavenging. Net community production and export in the central Arctic Ocean have been estimated using several approaches. We have already mentioned that export production measured with ^{234}Th/^{238}U and with ^{210}Po/^{210}Pb was very low in 2007 and 2011. New ^{234}Th data from 2015 show essentially no increase in export productivity (Black, 2018). In 2011, Ulfsbo et al. (2014) found enhanced net community production values on the shelves and ice margin, but in the central Arctic their O_2/Ar, pCO_2, and nutrient drawdown estimates are very low and do not appear to have increased in 2015 (Ulfsbo, pers. comm.).

Alternatively, the ice melt could have caused an increase of scavenging rate through the release of ice rafted particles that previously used to be carried on to Fram Strait.

Finally, the lower ^{228}Th/^{228}Ra ratios could result from a more rapid transport of the TPD. The IBTs of the Healy stations crossed the shelf break (200-m isobaths) 8–18 months before sampling (Kipp et al., 2018). For the *Polarstern* study this was 5–11 months, clearly shorter than the corresponding time for the IBTs of the 2007 study (7–27 months, Figure S3b). The observed trend (1992–2009) toward increasing ice drift speed has

been related to the thinning of the ice cover and to changed wind forcing (Spreen et al., 2011). The roughly 9 months shorter transport time in 2015 compared to 2007 would explain much less ingrowth of ^{228}Th into parent ^{228}Ra during transit (equation (4)) and 9% higher ^{228}Ra values as a result of less decay.

4.4. Depth Distribution of ^{228}Ra

The major source of ^{228}Ra in the central Arctic Ocean is the supply of shelf-derived water to the low-salinity surface layer. As a first approximation of the depth distribution we therefore use a one-dimensional model with a source of high ^{228}Ra concentrations in the surface mixed layer (depth MLD). Thereafter, the depth distribution is controlled by vertical diffusion (eddy diffusion coefficient k_z) and radioactive decay and follows an exponential decay.

$$A_R = A_{R^0} e^{-\sqrt{\frac{\lambda_R}{k_z}}(z-\mathrm{MLD})} \tag{5}$$

With this equation and using k_z of order 10^{-4} m^2 s^{-1} (Munk, 1966), ^{228}Ra falls below 1 dpm m^{-3} at 1,000 m and would be below our detection limit in deeper layers. ^{228}Ra is also released from the deep-sea floor. Close to the seafloor we observe activities up to 8.2 dpm m^{-3} (Sta. PS94–81). Even with a 10 times higher vertical diffusivity in the benthic boundary layer, this input would fall below 1 dpm m^{-3} at 1,100 m above the seafloor. Nevertheless, all intermediate water values are above our detection limit. The lowest activities observed on the PS94 expedition are down to 1.14 ± 0.31 dpm m^{-3} in the Makarov Basin (Sta. PS94–101 and Sta. PS94–96), but in the Eurasian Basin, all values are above 1.9 ± 0.4 dpm m^{-3}. The higher activities must be supplied by horizontal diffusion and advection from the slopes, similar to the situation observed during the GEOSECS program in the NW Atlantic (Sarmiento et al., 1982). In the Arctic Ocean, this process is enhanced by slope convection resulting from brine rejection during sea ice formation (Rudels et al., 2000). Analysis of the distribution of Al, Si (Middag et al., 2009), and Ba (Roeske et al., 2012) showed that shelf sources were a major contribution to the enrichment of these elements in the deep basins. We expect that slope convection contributes to Ra enrichment at all depths in a similar way.

Intermediate depth waters—particularly high subsurface ^{228}Ra activities—are observed in the Amundsen Basin down to approximately 1,500 m. The circulation of intermediate depth waters in the Arctic Ocean has been reviewed by Rudels (2015). Based on hydrographic (T, S, and Si) and CFC data, Rudels et al. (1994) showed how the Atlantic input splits into a Fram Strait Branch and a Barents Sea Branch. These branches meet north of the Kara Sea, and the resulting intermediate depth water mass is strongly affected by inputs from the shelves, via inputs to the Barents Sea Branch itself and through further sinking shelf plumes. These authors found a return flow of Atlantic water at 200–1,700 m in the Amundsen Basin with a residence time on the order of a decade ("the deeper layers being the oldest"). ^{228}Ra data collected in 1987 (Rutgers van der Loeff et al., 1995) gave the first evidence that this return flow had enhanced ^{228}Ra concentrations through its contact with the shelves. Samples taken from a submarine cruising at 132 m (Kadko & Aagaard, 2009) showed a maximum in the Amundsen Basin (their Sta. 6), thought to be derived from the Laptev or Kara Sea after a transit of at least 2 years based on estimates of Woodgate et al. (2001) that the water speed along the Eurasian side of the Lomonosov ridge is 2 cm/s.

Our new data collected in 2015 show clearly enhanced ^{228}Ra activities in intermediate waters up to about 1,500 m in the Amundsen Basin compared to the Nansen and Makarov Basin (Figure 6). At 1,000 m, we find 18 and 20 dpm m^{-3} at Stas PS94–81 and PS94–117, respectively, compared to only 5 dpm m^{-3} at Sta. PS94–101 in the Makarov Basin. SF_6 data on the PS94 transect (Figure 9, full section in Figure S4, data in Smethie, 2017; Smethie & Swift, 2018) across the Amundsen Basin show indeed that at the depth horizon of 1,000 m this basin is locally enriched at Sta. PS94–81 to >1.75 fmol/kg, corresponding to a ventilation age of 15–18 years, if before ventilation the surface water had reached equilibrium with the atmosphere. We assume that the Atlantic water mass carrying 20–30 dpm m^{-3} when entering the Arctic through the Barents Sea Opening and Fram Strait (Key et al., 1992) is enriched up to concentrations of order 150 dpm m^{-3} in the Kara and Laptev Sea (Rutgers van der Loeff et al., 2003), while the SF_6 content equilibrates with the atmosphere. In a purely advective transport of this water mass as intermediate water in the Amundsen Basin, the SF_6 content would remain unchanged, while ^{228}Ra would decay to the observed 18 dpm m^{-3} in 18 years, which means that the time scale of the two tracers matches. A further independent support for this time scale

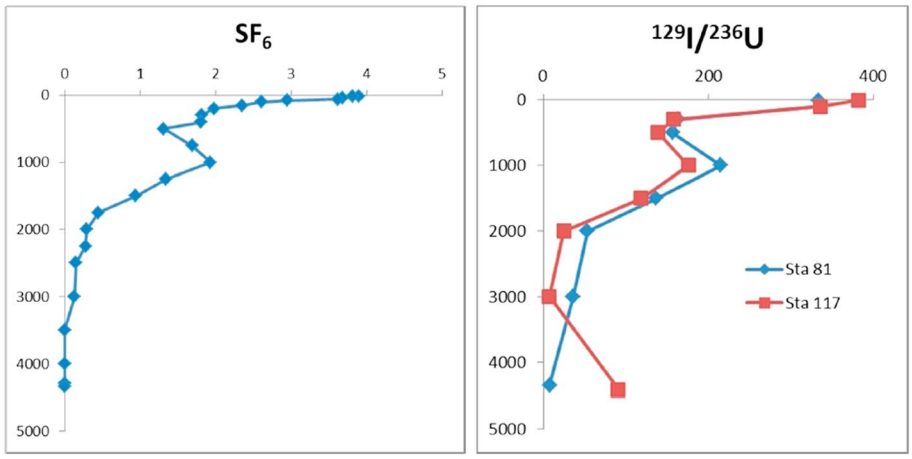

Figure 9. Depth profile of SF_6 (left, fmol/kg) at station PS94–81 and of $^{129}I/^{236}U$ (right, at/at) at station PS94–81 (blue) and PS94–117 (red) in the Amundsen Basin showing ventilation of the intermediate water up to about 1,500 m.

comes from the $^{129}I/^{236}U$ signal (Figure 9). The relatively high $^{129}I/^{236}U$ ratios of 215 and 176 for Stas PS94–81 and 117 observed at 1,000 m, respectively, could only be explained by waters that were released after 1998 by the European Reprocessing Plants of Sellafield and La Hague (Casacuberta et al., 2016; Christl et al., 2015). Although transit times using the $^{129}I/^{236}U$ atom ratio cannot yet be calculated as precisely as for SF_6, they would still generally agree with the ones estimated based on SF_6 and ^{228}Ra.

4.5. A Model of the Distribution of ^{228}Th, ^{228}Ra, and the $^{228}Th/^{228}Ra$ Ratio

A soluble parent with a particle reactive daughter with half-life of 1.9 years, the $^{228}Th/^{228}Ra$ tracer pair appears ideally suited as a tracer for export production in the Arctic where ^{228}Ra is abundant. Compared to the $^{234}Th/^{238}U$ tracer pair, the longer half-life has the advantage of averaging out short-term variations within the productive season, and it creates a much larger depletion relative to the soluble parent that can be determined with better precision. Here we model the vertical distribution of ^{228}Ra and ^{228}Th in order to investigate to what extent these tracers can be used to determine particle flux and export production.

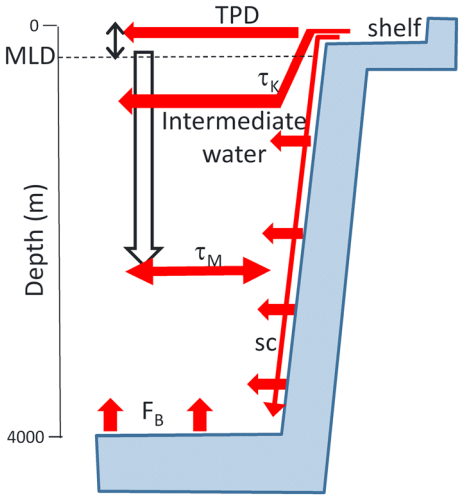

Figure 10. Profile model of the distribution of ^{228}Ra and ^{228}Th with rapid mixing down to the mixed layer depth (MLD), lateral input at the surface in the TPD, ventilation of the upper 1,500 m with shelf water from the Kara Sea (time scale τ_K), exchange at all depths with ^{228}Ra-enriched bottom waters at the slope (time scale τ_M) with ^{228}Ra-enrichment maintained by slope convection (sc), and an input F_B from the seafloor. The vertical particle flux (black arrow) carrying particulate ^{228}Th is modeled using data of ^{234}Th and ^{230}Th.

We use a profile model (Figure 10, equations provided in the supporting information) where ^{228}Ra and ^{228}Th are introduced in the surface layer. We represent the supply in the TPD by setting the activities of ^{228}Ra and ^{228}Th in the surface mixed layer (depth MLD) at fixed values $^{228}Ra°$ and $^{228}Th°$. Below the surface mixed layer, vertical eddy diffusion is set at 1.3 10^{-4} m^2 s^{-1} (Munk, 1966). ^{228}Ra release from the seafloor sediment causes an input F_B of 250 dpm m^{-2} yr^{-1} corresponding in steady state to a deep-water inventory of 2,000 dpm m^{-2}. Moreover, the supply of ^{228}Ra from slope sediments is represented as an exchange at all depths with a water mass at the margin with $^{228}Ra_M$ = 25 dpm m^{-3} and $^{228}Th_M$ = 10 dpm m^{-3} with time constant τ_M. To represent the special case of the Amundsen Basin, the water mass from MLD to 1,500 m is renewed with Kara Sea shelf water with composition $^{228}Ra_K$ and $^{228}Th_K$ with time constant τ_M. This input is balanced by outflow through FRAM Strait.

In the water column below depth MLD, ^{228}Ra decays with a half-life of 5.75 years to ^{228}Th, which decays with a half-life of 1.9 years. For ^{228}Th we use the reversible scavenging model of Nozaki et al. (1981) and Bacon and Anderson (1982) in which the particulate and dissolved forms are in continuous exchange with adsorption rate k_1 and desorption rate k_{-1}. We calculate these rate constants from observations of the

Table 1
Parameters of the Profile Model Representing ^{228}Ra and ^{228}Th

Parameter	Symbol	Value			Unit	Sensitivity analysis
		Nansen/Amundsen	Makarov	Canada		
Mixed layer (ML) depth	MLD		100		m	
Eddy diff coeff	k_z		4,100		$m^2\ yr^{-1}$	410–4,100
Benthic ^{228}Ra flux	F_B		250		dpm $m^{-2}\ yr^{-1}$	
^{228}Ra in ML	$^{228}Ra°$	157		55	dpm m^{-3}	
^{228}Th in ML	$^{228}Th°$	47		25	dpm m^{-3}	
^{228}Ra at margin	$^{228}Ra_M$		25		dpm m^{-3}	
^{228}Th at margin	$^{228}Th_M$		10		dpm m^{-3}	0–25
Exchange time with margin	τ_M		50		yr	1-inf.
^{228}Ra Kara Sea	$^{228}Ra_K$		150		dpm m^{-3}	
^{228}Th Kara Sea	$^{228}Th_K$		0		dpm m^{-3}	
C_p/C_d ^{230}Th [b]	K_{230}	0.5	0.152	0.152[a]	-.-	
C_p/C_d ^{234}Th [b]	K_{234}	0.12	0.026	0.026[a]	-.-	
Adsorption rate constant	k_1	1.59	0.324	0.324[a]	yr^{-1}	
Desorption rate constant	k_{-1}	3.18	2.132	2.132[a]	yr^{-1}	
C_d ^{230}Th at 4,000 m	$^{230}Th_{d,4000}$	0.35	1.55	1.55[a]	dpm m^{-3}	
Particle settling rate	S	582	434	434[a]	m yr^{-1}	
Exchange time with Kara Sea	τ_K	50	inf	inf	yr	1-inf.

[a]Assumed identical to Makarov. [b]Valk, pers. comm.

distribution of the Th isotopes ^{230}Th and ^{234}Th (Valk, pers. comm.). For every isotope, the ratio of particulate to dissolved Th is given by $C_p/C_d = k_1/(\lambda + k_{-1}$; equation (13) in Bacon & Anderson, 1982). From the ratio of particulate to dissolved activities of ^{230}Th and ^{234}Th in the deep Nansen Basin of 0.5 and 0.12, respectively, we find values for k_1 and k_{-1} of 1.6 and 3.2 yr^{-1}, respectively. Applying the reversible exchange model to the distribution of the long-lived isotope ^{230}Th, C_p increases linearly with depth z as C_p = Pd/S*z, where Pd is the ^{230}Th production rate and S is the particle sinking rate. From the distribution of ^{230}Th, with dissolved ^{230}Th increasing to 7.5 fg/kg (0.35 dpm m^{-3}) at 4,000 m in the Nansen/Amundsen Basin, we find a value for the average particle sinking rate S of 582 m yr^{-1}. For the Makarov Basin, where dissolved ^{230}Th increases to 33 fg/kg (1.55 dpm m^{-3}) at 4,000 m, we find rate constants k_1 and k_{-1} of 0.3 and 2.1 yr^{-1}, respectively, and a particle settling rate S of 434 m yr^{-1}.

The differential equations in the model (supporting information) were solved for ^{228}Ra and ^{228}Th in the water column below the surface mixed layer using programming language R based on scripts presented by Soetaert and Herman (2008). All parameters are listed in Table 1.

4.5.1. ^{228}Ra Model

The time scales of the lateral exchange processes with the slope (τ_M) and by ventilation with the Kara Sea (τ_K) are modified (Table 1) in order to obtain the best representation of the observed ^{228}Ra profiles. Without input from the slope, ^{228}Ra becomes practically zero from 2,000 to 4,000 m depth. With a margin exchange time of 50 years, ^{228}Ra in this depth range becomes 3.5 dpm m^{-3} (Figure 11a), which fits with observations. The best fit for ^{228}Ra in the intermediate water in the Amundsen Basin is found for a renewal time of intermediate water with Kara Sea surface water of 50 years. This yields a ^{228}Ra activity of 22 dpm m^{-3} at 1,000 m (Figure S5). This renewal time is longer than the pure decay time of 18 years found above because here we do not use a complete replacement of the water in a purely advective model but rather a continuous flushing of a well-mixed water mass.

4.5.2. ^{228}Th Model

If ^{228}Ra followed equation (5), that is, in the absence of lateral inputs, and if thorium were unreactive, that is, in the absence of scavenging in the water column ($\lambda_s = 0$) the activity of ^{228}Th (A_T) would be described by equation (6) in Rutgers van der Loeff et al. (2012)

$$A_T = \frac{\lambda_T A_{R^0}}{\lambda_T - \lambda_R} e^{-\sqrt{\frac{\lambda_R}{k_z}}(z-\mathrm{MLD})} + \left(A_{T^0} - \frac{\lambda_T A_{R^0}}{\lambda_T - \lambda_R}\right) e^{-\sqrt{\frac{\lambda_T}{k_z}}(z-\mathrm{MLD})} \quad (6)$$

and at great depth the activity ratio would approach

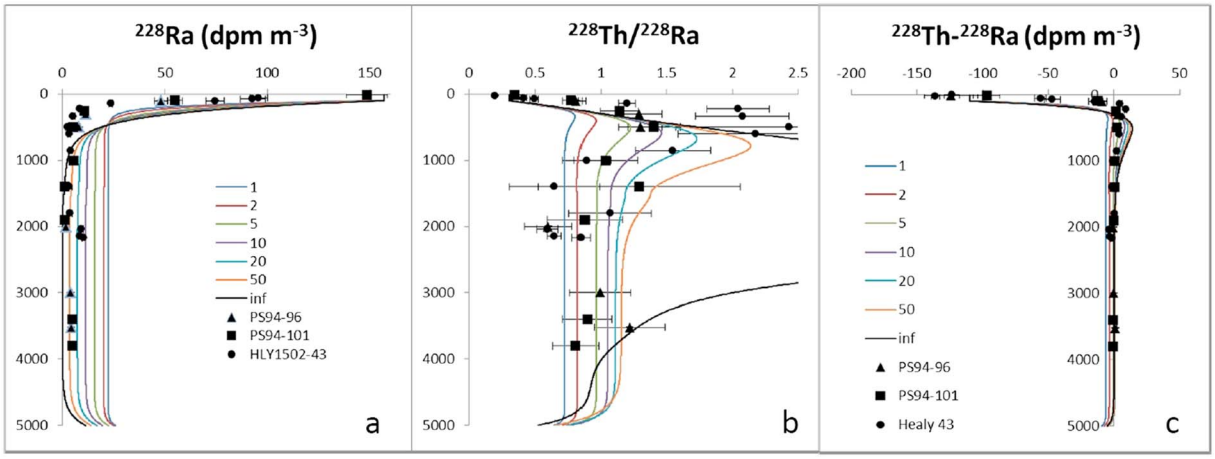

Figure 11. Model run for ^{228}Ra, ^{228}Th/^{228}Ra, and ^{228}Th-^{228}Ra in the Makarov Basin varying the time scale τ_M (years) for exchange with the margin. High ^{228}Ra values near 2,100 m at station HLY1502–43 are due to proximity to seafloor.

$$\frac{A_T}{A_R} \rightarrow \frac{\lambda_T}{\lambda_T - \lambda_R} = 1.49 \tag{7}$$

(cf. Rutgers van der Loeff et al., 2012, their Figure 11). Using our model for ^{228}Ra and the reversible exchange model for Th with rate constants determined for the Makarov Basin (Table 1), we find that the release of ^{228}Th from particles settling out of the mixed layer causes an enrichment of ^{228}Th over ^{228}Ra with a maximum AR of 2.14 at a depth of 780 m (Figures 11b and 12). At greater depth, the AR stabilizes at a value of 1.11. This result is in reasonable agreement with observations in the Makarov Basin (Stas PS94–96 and 101, HLY1502–43, Figures 11b and 12a).

We find that the distribution of ^{228}Th/^{228}Ra and of the excess ^{228}Th ($^{228}Th_{xs} = {}^{228}Th - {}^{228}Ra$) are very sensitive to the assumed parameters for the exchange with the margin (Figures 11b and 11c and 13). If no exchange is taken into account (exchange time scale infinity), ^{228}Ra will tend to zero at middepth and the ^{228}Th/^{228}Ra ratio increases to very high values. $^{228}Th_{xs}$ reaches the highest values at 510 m depth and is zero in the deep water. A rapid exchange with the margin (time scale 1 year) causes higher ^{228}Ra concentrations and lower ^{228}Th/^{228}Ra ratios. If we select the exchange rate of 50 years that best fits the observed ^{228}Ra profile and vary the degree of ^{228}Th/^{228}Ra disequilibrium (activity ratio AR_M) in the water mass at the margin that is the source for the lateral supply of ^{228}Ra, we find that especially the deepwater ^{228}Th/^{228}Ra ratio is strongly dependent on the ^{228}Th in the source water (Figure 12a). If the water at the margin is depleted in ^{228}Th by scavenging at the slope ($AR_M = 0$), the modeled $^{228}Th_{xs}$ at depth becomes negative (^{228}Th/^{228}Ra = 0.95). If however ^{228}Th is in equilibrium with ^{228}Ra in the margin water (we use $AR_M = 1$ and not 1.49 because of the proximity of ^{228}Ra to its ^{232}Th parent), the $^{228}Th_{xs}$ remains positive (^{228}Th/^{228}Ra = 1.31). The result for AR = 0.4, the value found at the Barents Slope by Cochran et al. (1995), is intermediate (^{228}Th/^{228}Ra = 1.15). This sensitivity analysis shows that the ^{228}Th/^{228}Ra ratio in the deepwater column (especially >1,500 m) is a delicate equilibrium between the lateral supply of ^{228}Ra and ^{228}Th and the vertical rain of particulate ^{228}Th. In the upper 1,000 m, the modeled ^{228}Th/^{228}Ra ratio is strongly dependent on the proper choice of the Ra inputs (Figure 11), but if the ^{228}Ra profile is properly resolved with good measurements of ^{228}Ra, the measured $^{228}Th_{xs}$ is only slightly dependent on the assumptions of the composition of the margin water (Figure 12b). This implies that the cumulative $^{228}Th_{xs}$ in the upper 1,500 m does not depend on lateral supply. The excess does depend on the inherent excess resulting from a parent/daughter pair where the decay of the parent is significant (equations (6) and (7)). This contribution can be estimated by setting the settling rate S at 0 (dashed line in Figures 12b and 12c).

In our model, the $^{228}Th_{xs}$ integrated from the depth where it becomes positive down to 1,500 m amounts to 7,700 dpm m^{-2} (varying between 6,900 and 8,400 dpm m^{-2} if AR_M is varied between 0 and 1), while in the absence of particle flux, the excess is only 1,500 dpm m^{-2}. At Stas PS94–96, PS94–101, and HLY1502–43 we

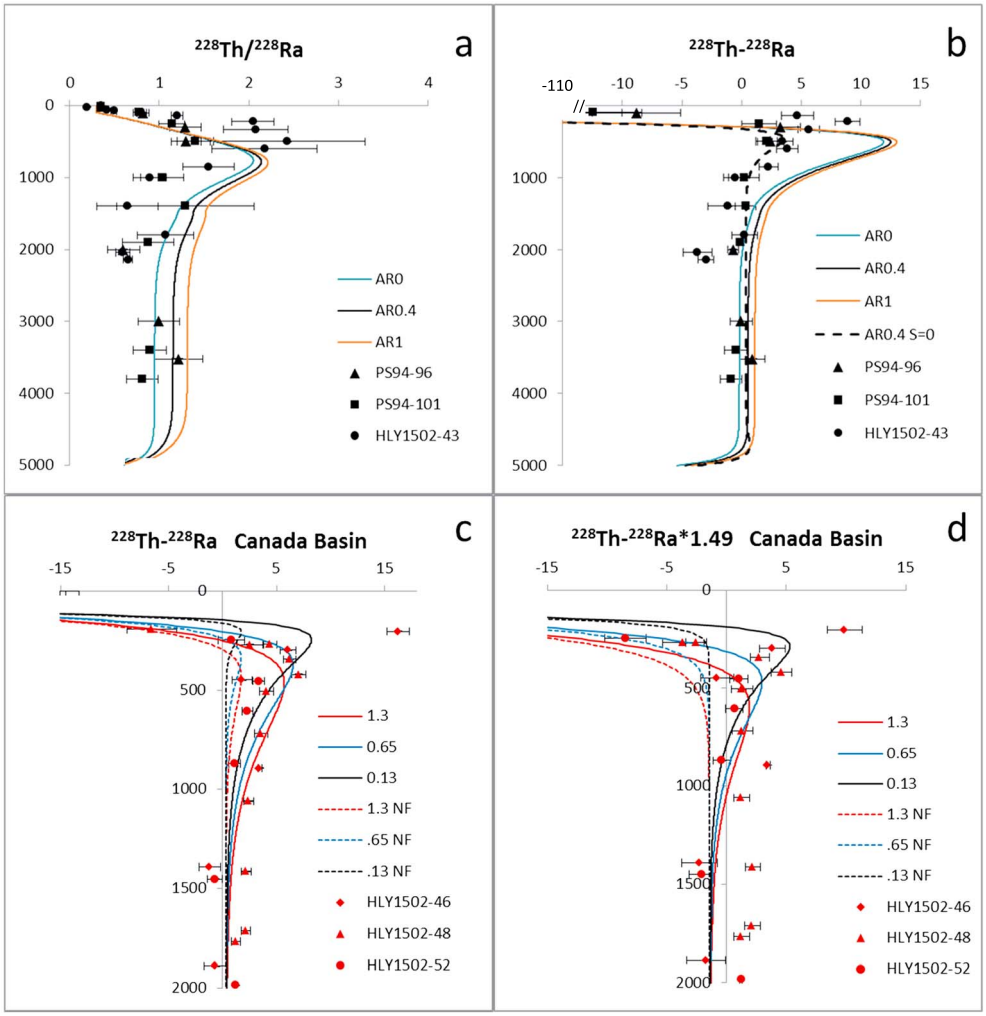

Figure 12. Depth distribution of (a) $^{228}Th/^{228}Ra$ ratio and (b) $^{228}Th_{xs}$ (dpm m^{-3}) using model parameters for the Makarov Basin, an exchange time with the margin of 50 years and $^{228}Th/^{228}Ra$ activity ratio at the margin (AR_M) varying between 0 and 1. Dashed line in (b): modeled $^{228}Th_{xs}$ (AR_M = 0.4) without particle flux. (c) ^{228}Th-^{228}Ra (based on ^{224}Ra-^{228}Ra) and (d) ^{228}Th-1.49*^{228}Ra (dpm m^{-3}) in the Canada Basin compared with model results with (full lines) and without (NF, dashed lines) particle flux, for the standard (1.3 10^{-4} m^2 s^{-1}) and two reduced values (0.65 10^{-4} and 0.13 10^{-4} m^2 s^{-1}) of the vertical diffusion coefficient k_z, using surface activities of ^{228}Ra and ^{228}Th of 55 and 25 dpm m^{-3}, respectively, and for further parameters the same values as in (a) and (b). ^{224}Ra data used as analogue for ^{228}Th in all data points.

found an integrated $^{228}Th_{xs}$ of 2,040 ± 900, 1,160 ± 550, and 3,400 ± 440 dpm m^{-2} (Figure 12b), not or not much exceeding the zero-particle-flux estimate.

In the Canada Basin, south of the core of the TPD, ^{228}Ra in surface water is much lower, which reduces the theoretical diffusive (i.e., zero-particle-flux) contribution to the ^{228}Th excess. At GN01 Stas HLY1502–46, 48, and 52, ^{228}Ra and ^{228}Th are on average 55 and 25 dpm m^{-3}, respectively. Using for the other parameters the same choice as in the Makarov Basin, we expect a ^{228}Th excess of 3,650 dpm m^{-2} compared to a zero-flux excess of 910 dpm m^{-2} (Figure 12c). The ^{228}Th excess actually observed agrees at Stas HLY1502–46 and 48 (3,710 ± 850 and 4,260 ± 210 dpm m^{-2}) with this estimate, while the excess observed at Sta HLY1502–52 (1,510 ± 330 dpm m^{-2}) only slightly exceeds the zero-flux estimate.

The maximum excess is observed at shallower depth than our model predicts. We may have overestimated the vertical diffusion coefficient, which is strongly reduced in the highly stratified surface layers of the Arctic Ocean. Figure 12c shows the sensitivity of the model results for the vertical diffusion coefficient k_z. A reduction of k_z by a factor of 2 or 10 does not affect the total predicted ^{228}Th excess, but it shifts the maximum

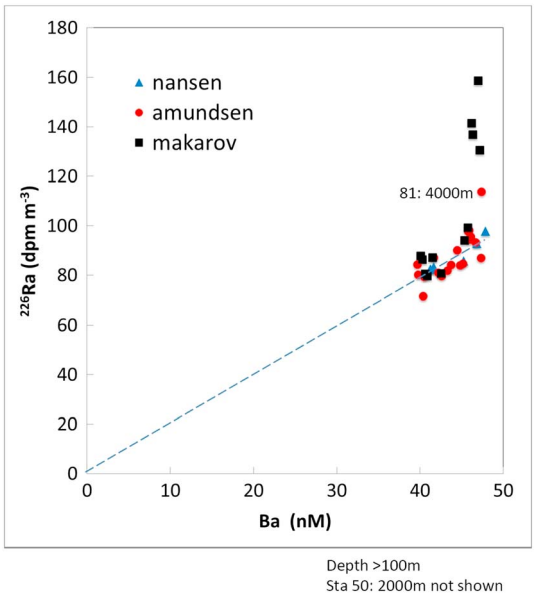

Figure 13. ^{226}Ra as function of Ba for all PS94 data in excess of 100 m depth showing that the accumulation of ^{226}Ra in deep water of the Makarov Basin is not associated with an accumulation of Ba. One unlikely data point of station PS94–50 (2,000 m) not shown.

excess to shallower depth. At the same time, it reduces the zero-flux-estimate of the cumulative excess from 910 to 780 or 604 dpm m^{-2}, respectively (Figure 12c).

An alternative way to take the inherent ^{228}Th excess in the unsupported ^{228}Ra decay chain into account is by plotting ^{228}Th-1.49*^{228}Ra (Figure 12d). The zero flux model results no longer show a subsurface maximum. The asymptotic value of (^{228}Th-1.49*^{228}Ra) approached at depth in the model results of Figure 12d is negative as a result of the lateral supply included in the model. When we integrate (^{228}Th-1.49*^{228}Ra) from the depth where it becomes positive down to 1,500 m, we find 2,048 ± 614, 2,094 ± 296, and 192 ± 170 dpm m^{-2} for Stas HLY1502–46, 48, and 52, respectively. In the Makarov Basin we find 1,476 ± 306 dpm m^{-2} at Sta HLY1502–43, while ^{228}Th never exceeds 1.49*Ra at stations PS94–96 and 101 (Table 2). These excess inventories at depth can be compared with the depletion of ^{228}Th in the surface water, roughly (^{228}Ra-^{228}Th)*MLD, which amounts to 11,000 and 3,000 dpm m^{-2} in the Makarov and Canada Basin, respectively (Table 1). We conclude that the ^{228}Th depletion in the Makarov Basin is largely advected in the TPD and not related to local particle export, whereas at Stas HLY1502–46, and 48 in the Canada Basin local export accounts for a larger part of the depletion and advection is of less importance.

Assuming steady state, the excess inventories can be converted to the vertical ^{228}Th flux (multiplying by λ_T) and then to the scavenging rate in the mixed layer (dividing by the ^{228}Th inventory in the MLD, Table 2). These results will be used in a subsequent paper dealing with carbon export fluxes.

4.6. ^{226}Ra and Deep Water Ventilation

It is tempting to use the accumulation of ^{226}Ra as an independent approach to estimate residence times of deep waters in the Arctic Basins. Broecker and Peng (1982) discussed the accumulation of ^{226}Ra in the deep waters of the World Ocean, based on data collected in the GEOSECS program. They considered that the accumulation was due to remineralization of ^{226}Ra from settling particles and to inputs from decay of ^{230}Th in deep-sea sediments. In principle, the two sources could be separated using Ba as analogue for a stable isotope of Ra, but they showed that in a two-layer ocean model the expected accumulation of the ^{226}Ra/Ba ratio in the deep sea due to the bottom source of ^{226}Ra was very small. The observed changes with very high accumulations in the deep NW Pacific were interpreted as result of inhomogeneities in the bottom source and in regeneration, making its use as deepwater ventilation tracer problematic. These problems are less restrictive in the Arctic Ocean with its relatively small and enclosed deep basins. Limited data on ^{230}Th$_{xs}$ activities in surface sediments (Hoffmann et al., 2013; Moran et al., 2005) show a general pattern of higher activities in the low productivity, permanently ice-covered interior Arctic, with average ^{230}Th$_{xs}$ in the upper 10 cm of the sediment of 9.9 dpm g^{-1} for the Nansen Basin (AOS94 core BC 32, 3,471 m) and 13.2 dpm g^{-1} for the Makarov

Table 2
*Integrated Values of (^{228}Th-^{228}Ra*1.49) and Corresponding Vertical ^{228}Th Flux and Scavenging Rate λ_s* in the Mixed Layer

Station	MLD	^{228}Ra$_{MLD}$	^{228}Th$_{MLD}$	Σ(^{228}Th-^{228}Ra*1.49)[a]100–1,500 m	±	Flux	τ_s	λ_s
	m	dpm m^{-3}	dpm m^{-3}	dpm m^{-2}		dpm m^{-2}yr^{-1}	yr	yr^{-1}
PS94–96	100	157	47	-.-		-.-		
PS94–101	100	157	47	-.-		-.-		
1502–43	100	157	47	1,476	306	538	8.7	0.11
1502–46	100	55	25	2,048	614	747	3.3	0.30
1502–48	100	55	25	2,094	296	764	3.3	0.31
1502–52	100	55	25	192	170	70	35.7	0.03

Note. -.-: no positive values.
[a]Positive values only.

Basin (BC 20, 3145 m; Hoffmann et al., 2013). The influence of remineralization on the accumulation of ^{226}Ra in the water column can be judged from a plot of ^{226}Ra versus Ba (Figure 12, Rember, 2017). Apart from a single data point at 4,000 m in the Amundsen Basin at Sta PS94–81, data from the deep Eurasian Basin do not stand apart from the general ^{226}Ra/Ba correlation and we conclude that in the Eurasian Basins the accumulation of ^{226}Ra cannot be unequivocally attributed to sediment sources. In the Makarov Basin, however, the accumulation of ^{226}Ra is not associated with a corresponding accumulation of Ba. In this case, as in the case of the ^{226}Ra accumulation observed at the Alpha Ridge by Moore and Smith (1986), we conclude that ^{226}Ra accumulation is due to release from bottom sediments. Following Cochran (1980) we estimate the ^{226}Ra release rate $F_{B,226}$ from the ^{230}Th inventory in the upper layer of the sediment. Using a ^{230}Th concentration of 14.8 dpm g^{-1}, a mixed layer of 8 cm as used by Cochran (1980), and a dry bulk density of 0.5 g dry material per cm^3 of sediment, we find a ^{226}Ra flux of 176 dpm m^{-2} yr^{-1}. This flux estimate varies between 156 and 180 dpm m^{-2} yr^{-1} if we allow for the range of mixed layer depths reported for AOS94 cores (2–10 cm, Smith et al., 2003). This flux must be balanced by decay and ventilation:

$$F_{B,226} = (\lambda_{226} + 1/\tau_{MD})\, I_{226} \tag{8}$$

where λ_{226} is the decay constant of ^{226}Ra, τ_{MD} is the residence time of water in the deep Makarov Basin, and I_{226} is the inventory of excess ^{226}Ra in the deep water. With the inventory derived above (70,000 dpm m^{-2}, Figure 7) we find a deepwater residence time of ~480 years, which is consistent with the estimated isolation age for the deep Canada and Makarov Basin of 450 years based on ^{14}C and ^{39}Ar (Schlosser et al., 1994; Schlosser et al., 1997).

5. Conclusions

When plotted as function of fraction meteoric water, ^{228}Ra has increased in the TPD from 2007 through 2011 to 2015. This change is most likely due to increased wave action on the shelves as a result of the longer ice free season. Whether the increase in ^{228}Ra flux is associated with increased fluxes of other terrigenous components requires continued studies of the ratio of these components to ^{228}Ra. The concomitant decrease of the ^{228}Th/^{228}Ra ratio likely results from a more rapid transit of surface waters depleted on the shelf and consequently less time for ingrowth of ^{228}Th.

In the TPD, particulate ^{228}Th accounts for most of the dissolved ^{224}Ra$_{xs}$. This implies a concept of excess ^{224}Ra that is very different from common use, that is, in most studies of coastal mixing ^{224}Ra$_{xs}$ is assumed to be derived only from the shelf such that (particulate) ^{228}Th is rarely considered of importance.

From the ^{228}Ra activity in the intermediate water in the Amundsen Basin (200–1,500 m) we derive a time scale for ventilation with shelf water derived from the Barents Sea Branch Water of about 18 years, in good agreement with estimates based on transient tracers SF$_6$ and ^{129}I/^{236}U.

The ratio ^{228}Th/^{228}Ra can be used in addition to ^{234}Th/^{238}U and ^{210}Po/^{210}Pb as a measure of export production in the Arctic Ocean. In the surface ocean, the depletion of ^{228}Th relative to its parent ^{228}Ra is widespread and it can be measured with higher precision than disequilibria of ^{234}Th/^{238}U and ^{210}Po/^{210}Pb, which are often very small in Arctic surface waters. The long time period has the advantage that removal over more than a full season is integrated, but it has the disadvantage that a large part of the disequilibrium is advected. The interpretation thus requires consideration of both advection and export (Rutgers van der Loeff et al., 2012).

In deep waters (>1,500 m) the ^{228}Th/^{228}Ra ratio is a delicate balance between the horizontal supply of ^{228}Ra and ^{228}Th by mixing with the slope and the vertical supply of ^{228}Th on sinking particles. In this depth range the ratio is an inappropriate tool to determine particle fluxes.

In subsurface waters, down to approx. 1,500 m, ^{228}Th accumulates up to a ^{228}Th/^{228}Ra ratio of about 2. This ^{228}Th$_{xs}$ is in part due to the small difference between the half-lives of ^{228}Ra and ^{228}Th (equations (5) and (6)), leaving barely any significant export flux of ^{228}Th in some stations (PS94–96, PS94–101, and HLY1502–52), but in others (HLY1502–43, 46, and 48), we find a significant export flux. Comparison with the depletion in the surface water shows that in the Makarov Basin this depletion is largely advected and must represent

export on the shelf where the water originated. At two stations in the Canada Basin such advection is less important and the export flux explains the larger part of the surface water depletion.

However, when this intermediate water mass is influenced by ventilation with the shelf (as is the case in the Amundsen Basin), the $^{228}Th/^{228}Ra$ signal in this depth range (100–1,500 m) depends critically on the $^{228}Th/^{228}Ra$ ratio in the ventilating shelf water mass, reducing its suitability as a tracer for export production.

The lack of coherence between ^{226}Ra and Ba in the deep Makarov Basin shows that the accumulation of ^{226}Ra here is not due to vertical particle flux but can be associated with release from bottom sediments. From a ^{226}Ra balance we estimate a deepwater residence time of about 480 years, which is consistent with the published estimates based on other tracers.

Data

The data used in this paper are provided in the supporting information and, where indicated, in the PANGAEA database (www.pangaea.de). ^{228}Ra and ^{226}Ra data of the HLY1502 expedition can be found at https://www.bco-dmo.org/dataset/718440.

Acknowledgments
We thank captain Schwarze with his crew of RV *Polarstern* and captain and crew of USCSC Healy for making this joint GEOTRACES study in the central Arctic Ocean a success. We are indebted to the chief scientists Ursula Schauer, David Kadko, and William Landing for their great support. Kai Uwe Ludwichowski and Jan van Ooijen provided the nutrient analyses during *Polarstern* expeditions PS78 and PS94. Virginie Sanial made us aware of a typo in equation (4). Mariele Paiva helped at the AWI lab to adjust the RaDeCC method for use with cartridges. We thank Ken Buesseler for his part in the ^{228}Th analyses. Many figures were produced with the software Ocean Data View (Schlitzer, 2017). We acknowledge funding from U.S. National Science Foundation (NSF) for U.S. GEOTRACES Ra isotope data (US NSF awards OCE-1458305 to Matthew Charette and OCE-1458424 to Willard Moore) and for SF6 measurements (US NSF grant OCE-1433922 to William Smethie). The paper benefitted from very constructive comments of Doug Hammond and an anonymous reviewer.

References

Aksenov, Y., Karcher, M., Proshutinsky, A., Gerdes, R., de Cuevas, B., Golubeva, E., et al. (2016). Arctic pathways of Pacific water: Arctic Ocean model intercomparison experiments. *Journal of Geophysical Research: Oceans*, *121*, 27–59. https://doi.org/10.1002/2015JC011299

Arrigo, K. R., Dijkin, G. V., & Pabi, S. (2008). Impact of a shrinking Arctic ice cover on marine primary production. *Geophysical Research Letters*, *35*, L19603. https://doi.org/10.1029/2008GL035028

Arrigo, K. R., Perovich, D. K., Pickart, R. S., Brown, Z. W., van Dijken, G. L., Lowry, K. E., et al. (2012). Massive phytoplankton blooms under Arctic Sea ice. *Science*, *336*(6087), 1408. https://doi.org/10.1126/science.1215065

Bacon, M. P., & Anderson, R. F. (1982). Distribution of thorium isotopes between dissolved and particulate forms in the deep sea. *Journal of Geophysical Research*, *87*(C3), 2045–2056. https://doi.org/10.1029/JC087iC03p02045

Bacon, M. P., Huh, C.-A., & Moore, R. M. (1989). Vertical profiles of some natural radionuclides over the alpha ridge, Arctic Ocean. *Earth and Planetary Science Letters*, *95*(1-2), 15–22. https://doi.org/10.1016/0012-821X(89)90164-7

Black, E. E. (2018). An investigation of basin-scale controls on upper ocean export and remineralization, (PhD thesis). MIT-WHOI Joint Program, Woods Hole, MA. https://doi.org/10.1575/1912/9576

Boetius, A., Albrecht, S., Bakker, K., Bienhold, C., Felden, J., Fernández-Méndez, M., et al. (2013). Export of algal biomass from the melting Arctic Sea ice. *Science*, *339*(6126), 1430–1432. https://doi.org/10.1126/science.1231346

Broecker, W. S., & Peng, T.-H. (1982). Tracers in the sea. Lamont- Doherty Geol. Obs., Columbia University.

Cai, P., Rutgers van der Loeff, M., Stimac, I., Nöthig, E.-M., Lepore, K., & Moran, S. B. (2010). Low export flux of particulate organic carbon in the central Arctic Ocean as revealed by ^{234}Th:^{238}U disequilibrium. *Journal of Geophysical Research*, *115*, C10037. https://doi.org/10.1029/2009JC005595

Casacuberta, N., Masqué, P., Henderson, G., Rutgers van der Loeff, M., Bauch, D., Vockenhuber, C., et al. (2016). First 236U data from the Arctic Ocean and use of 236U/238U and 129I/236U as a new dual tracer. *Earth and Planetary Science Letters*, *440*, 127–134.

Charette, M. A., Dulaiova, H., Gonneea, M. E., Henderson, P. B., Moore, W. S., Scholten, J. C., & Pham, M. K. (2012). GEOTRACES radium isotopes interlaboratory comparison experiment. *Limnology and Oceanography: Methods*, *10*(6), 451–463. https://doi.org/10.4319/lom.2012.10.451

Charkin, A. N., Rutgers van der Loeff, M., Shakhova, N. E., Gustafsson, Ö., Dudarev, O. V., Cherepnev, M. S., et al. (2017). Discovery and characterization of submarine groundwater discharge in the Siberian Arctic seas: A case study in the Buor-Khaya Gulf, Laptev Sea. *The Cryosphere*, *11*(5), 2305–2327. https://doi.org/10.5194/tc-11-2305-2017

Christl, M., Casacuberta, N., Vockenhuber, C., Elsässer, C., Bailly du Bois, P., Herrmann, J., & Synal, H.-A. (2015). Reconstruction of the 236U input function for the Northeast Atlantic Ocean: Implications for 129I/236U and 236U/238U-based tracer ages. *Journal of Geophysical Research: Oceans*, *120*, 7282–7299. https://doi.org/10.1002/2015JC011116

Cochran, J. K. (1980). The flux of 226Ra from deep-sea sediments. *Earth and Planetary Science Letters*, *49*(2), 381–392. https://doi.org/10.1016/0012-821X(80)90080-1

Cochran, J. K., Hirschberg, D. J., Livingston, H. D., Buesseler, K. O., & Key, R. M. (1995). Natural and anthropogenic radionuclide distributions in the Nansen Basin, Arctic Ocean: Scavenging rates and circulation time scales. *Deep-Sea Research Part II*, *42*(6), 1495–1517. https://doi.org/10.1016/0967-0645(95)00051-8

Cutter, G., Andersson, P., Codispoti, L., Croot, P., Francois, R., Lohan, M., et al. (2010). Sampling and sample-handling protocols for GEOTRACES cruises—Version 1. GEOTRACES (98 pp.).

Elsinger, R. J., King, P. T., & Moore, W. S. (1982). Radium-224 in natural waters measured by g ray spectrometry. *Analytica Chimica Acta*, *144*, 277–281. https://doi.org/10.1016/S0003-2670(01)95545-X

Grosfeld, K., Treffeisen, R., Asseng, J., Bartsch, A., Bräuer, B., Fritzsch, B., et al. (2016). Online sea-ice knowledge and data platform. *Polarforschung*, *85*, 143–155.

Günther, F., Overduin, P. P., Sandakov, A. V., Grosse, G., & Grigoriev, M. N. (2013). Short- and long-term thermo-erosion of ice-rich permafrost coasts in the Laptev Sea region. *Biogeosciences*, *10*(6), 4297–4318. https://doi.org/10.5194/bg-10-4297-2013

Henderson, P. B., Morris, P. J., Moore, W. S., & Charette, M. A. (2013). Methodological advances for measuring low-level radium isotopes in seawater. *Journal of Radioanalytical and Nuclear Chemistry*, *296*(1), 357–362. https://doi.org/10.1007/s10967-012-2047-9

Hoffmann, S. S., McManus, J. F., Curry, W. B., & Brown-Leger, L. S. (2013). Persistent export of 231Pa from the deep central Arctic Ocean over the past 35,000 years. *Nature*, *497*(7451), 603–606. https://doi.org/10.1038/nature12145

Kadko, D., & Aagaard, K. (2009). Glimpses of Arctic Ocean shelf-basin interaction from submarine-borne radium sampling. *Deep Sea Research, Part I*, *56*(1), 32–40. https://doi.org/10.1016/j.dsr.2008.08.002

Kadko, D., & Landing, W. (2015). U.S. Arctic GEOTRACES USCGC Healy (HLY1502) cruise report. Retrieved from https://www.bodc.ac.uk/resources/inventories/cruise_inventory/reports/healy1502.pdf

Kadko, D., & Muench, R. (2005). Evaluation of shelf-basin interaction in the western Arctic by use of short-lived radium isotopes: The importance of mesoscale processes. *Deep Sea Research Part II: Topical Studies in Oceanography*, *52*(24-26), 3227–3244. https://doi.org/10.1016/j.dsr2.2005.10.008

Karcher, M. J., Smith, J. N., Kauker, F., Gerdes, R., & Smethie, W. M. Jr. (2012). Recent changes of Arctic Ocean circulation revealed by 129 iodine observations and modelling. *Journal of Geophysical Research*, *117*, C08007. https://doi.org/10.1029/2011JC007513

Key, R. M., Moore, W. S., & Sarmiento, J. L. (1992). Transient tracers in the Ocean North Atlantic Study. Final Data Report for ^{228}Ra and ^{226}Ra (193 pp.). Princeton, NJ: Ocean Tracer Laboratory.

Kipp, L. E., Charette, M. A., Moore, W. S., Henderson, P. B., & Rigor, I. G. (2018). Increased fluxes of shelf-derived materials to the central Arctic Ocean. *Science Advances*, *4*(1), eaao1302. https://doi.org/10.1126/sciadv.aao1302

Klunder, M. B., Bauch, D., Laan, P., Baar, H. J. W. D., Heuven, S.v., & Ober, S. (2012). Dissolved iron in the Arctic shelf seas and surface waters of the central Arctic Ocean: Impact of Arctic river water and ice-melt. *Journal of Geophysical Research*, *117*, C01027. https://doi.org/10.01029/02011JC007133

Krumpen, T. (2017). ICETrack: Antarctic and Arctic Sea ice monitoring and tracking tool—User guide (pp. 1–14). Bremerhaven: AWI.

Laukert, G., Frank, M., Bauch, D., Hathorne, E. C., Gutjahr, M., Janout, M., & Hölemann, J. (2017). Transport and transformation of riverine neodymium isotope and rare Earth element signatures in high latitude estuaries: A case study from the Laptev Sea. *Earth and Planetary Science Letters*, *477*, 205–217. https://doi.org/10.1016/j.epsl.2017.08.010

Li, Y.-H., Feely, H. W., & Toggweiler, J. R. (1980). ^{228}Ra and ^{228}Th concentrations in GEOSECS Atlantic surface waters. *Deep Sea Research*, *27A*, 545–555.

Luo, D., Wu, Q., Jin, H., Marchenko, S. S., Lü, L., & Gao, S. (2016). Recent changes in the active layer thickness across the northern hemisphere. *Environmental Earth Sciences*, *75*(7), 555. https://doi.org/10.1007/s12665-015-5229-2

Luo, S., Ku, T.-L., Kusakabe, M., Bishop, J. K. B., & Yang, Y.-L. (1995). Tracing particle cycling in the upper ocean with ^{230}Th and ^{228}Th: An investigation in the equatorial Pacific along 140°W. *Deep Sea Research, Part II*, *42*(2-3), 805–829. https://doi.org/10.1016/0967-0645(95)00019-M

Maiti, K., Charette, M. A., Buesseler, K. O., Zhou, K., Henderson, P., Moore, W. S., et al. (2014). Determination of particulate and dissolved 228Th in seawater using a delayed coincidence counter. *Marine Chemistry*. https://doi.org/10.1016/j.marchem.2014.12.001

McClelland, J. W., Holmes, R. M., Dunton, K. H., & Macdonald, R. W. (2012). The Arctic Ocean estuary. *Estuaries and Coasts*, *35*(2), 353–368. https://doi.org/10.1007/s12237-010-9357-3

Middag, R., de Baar, H. J. W., Laan, P., & Bakker, K. (2009). Dissolved aluminium and the silicon cycle in the Arctic Ocean. *Marine Chemistry*, *115*(3-4), 176–195. https://doi.org/10.1016/j.marchem.2009.08.002

Middag, R., de Baar, H. J. W., Laan, P., & Klunder, M. B. (2011). Fluvial and hydrothermal input of manganese into the Arctic Ocean. *Geochimica et Cosmochimica Acta*, *75*(9), 2393–2408. https://doi.org/10.1016/j.gca.2011.02.011

Moore, R. M., & Smith, J. N. (1986). Disequilibria between ^{226}Ra, ^{210}Pb and ^{210}Po in the Arctic Ocean and the implications for the chemical modification of the Pacific water inflow. *Earth and Planetary Science Letters*, *77*(3-4), 285–292. https://doi.org/10.1016/0012-821X(86)90140-8

Moore, W. S. (1984). Radium isotope measurements using germanium detectors. *Nuclear Instruments and Methods in Physics Research*, *223*(2-3), 407–411. https://doi.org/10.1016/0167-5087(84)90683-5

Moore, W. S. (1996). Large groundwater inputs to coastal waters revealed by ^{226}Ra enrichments. *Nature*, *380*(6575), 612–614. https://doi.org/10.1038/380612a0

Moore, W. S., & Arnold, R. (1996). Measurement of ^{223}Ra and ^{224}Ra in coastal waters using a delayed coincidence counter. *Journal of Geophysical Research*, *101*, 1321–1329. https://doi.org/10.1029/95JC03139

Moore, W. S., Sarmiento, J. L., & Key, R. M. (2008). Submarine groundwater discharge revealed by ^{228}Ra distribution in the upper Atlantic Ocean. *Nature Geoscience*, *1*(5), 309–311. https://doi.org/10.1038/ngeo183

Moran, S. B., Shen, C.-C., Edwards, L. R., Edmonds, H. N., Scholten, J. C., Smith, J. N., & Ku, T.-L. (2005). ^{231}Pa and ^{230}Th in surface sediments of the Arctic Ocean: Implications for ^{231}Pa/^{230}Th fractionation, boundary scavenging, and advective export. *Earth and Planetary Science Letters*, *234*(1-2), 235–248. https://doi.org/10.1016/j.epsl.2005.02.016

Munk, W. (1966). Abyssal recipes. *Deep Sea Research*, *13*, 707–730.

Nozaki, Y., Horibe, Y., & Tsubota, H. (1981). The water column distributions of thorium isotopes in the western North Pacific. *Earth and Planetary Science Letters*, *54*(2), 203–216. https://doi.org/10.1016/0012-821X(81)90004-2

Rabe, B., Karcher, M., Kauker, F., Schauer, U., Toole, J. M., Krishfield, R. A., et al. (2014). Arctic Ocean basin liquid freshwater storage trend 1992–2012. *Geophysical Research Letters*, *41*, 961–968. https://doi.org/10.1002/2013GL058121

Rember, R. (2017). PS94 Ba data. Retrieved from www.pangaea.de

Roca-Martí, M., Puigcorbé, V., Rutgers van der Loeff, M., Katlein, C., Fernández-Méndez, M., Peeken, I., & Masqué, P. (2016). Carbon export fluxes and export efficiency in the central Arctic during the record sea-ice minimum in 2012: A joint 234Th/238U and 210Po/210Pb study. *Journal of Geophysical Research: Oceans*, *121*, 5030–5049. https://doi.org/10.1002/2016JC011816

Roeske, T., Middag, R., Bakker, K., & Rutgers van der Loeff, M. (2012). Deep water circulation and shelf water inputs to the Arctic Ocean by dissolved Ba. *Marine Chemistry*, *132–133*, 56–67. https://doi.org/10.1016/j.marchem. 2012.1002.1001

Rudels, B. (2015). Arctic Ocean circulation, processes and water masses: A description of observations and ideas with focus on the period prior to the international polar year 2007–2009. *Progress in Oceanography*, *132*, 22–67. https://doi.org/10.1016/j.pocean.2013.11.006

Rudels, B., Jones, E. P., Anderson, L. G., & Kattner, G. (1994). On the intermediate depth waters of the Arctic Ocean. In O. M. Johannessen, R. D. Muench, & J. E. Overland (Eds.), *The polar oceans and their role in shaping the global environment: The Nansen centennial volume*, *Geophysical Monograph* (Vol. 85, pp. 33–46). Washington, DC: American Geophysical Union.

Rudels, B., Muench, R. D., Gunn, J., Schauer, U., & Friedrich, H. J. (2000). Evolution of the Arctic Ocean boundary current north of the Siberian shelves. *Journal of Marine Systems*, *25*(1), 77–99. https://doi.org/10.1016/S0924-7963(00)00009-9

Rutgers van der Loeff, M., Cai, P., Stimac, I., Bauch, D., Hanfland, C., Roeske, T., & Bradley Moran, S. (2012). Shelf-basin exchange times of Arctic surface waters estimated from ^{228}Th/^{228}Ra disequilibrium. *Journal of Geophysical Research*, *117*, C03024. https://doi.org/10.01029/02011JC007478

Rutgers van der Loeff, M., Kuhne, S., Wahsner, M., Holtzen, H., Frank, M., Ekwurzel, B., et al. (2003). ^{228}Ra and ^{226}Ra in the Kara and Laptev seas. *Continental Shelf Research*, *23*(1), 113–124. https://doi.org/10.1016/S0278-4343(02)00169-3

Rutgers van der Loeff, M. M., Key, R. M., Scholten, J. C., Bauch, D., & Michel, A. (1995). ^{228}Ra as a tracer for shelf water in the Arctic Ocean. *Deep-Sea Research Part II*, *42*(6), 1533–1553. https://doi.org/10.1016/0967-0645(95)00053-4

Sarmiento, J. L., Rooth, C. G. H., & Broecker, W. S. (1982). Radium 228 as a tracer of basin wide processes in the abyssal ocean. *Journal of Geophysical Research*, *87*, 9694–9698. https://doi.org/10.1029/JC087iC12p09694

Schauer, U. (2012). The expedition of the research vessel "Polarstern" to the Arctic in 2011 (ARK-XXVI/3-TransArc). Reports on polar and marine research 649 (205 pp.).

Schauer, U. (2016). The Expedition PS94 of the research vessel POLARSTERN to the central Arctic Ocean in 2015, Bremerhaven, Alfred Wegener Institute for Polar and Marine Research. Berichte zur Polar- und Meeresforschung = Reports on polar and marine research 703 170 pp.

Schlitzer, R. (2017). Ocean data view. Retrieved from http://odv.awi.de

Schlosser, P., Kromer, B., Ekwurzel, B., Bönisch, G., McNichol, A., Schneider, R., et al. (1997). The first trans-Arctic 14C section: Comparison of the mean ages of the deep waters in the Eurasian and Canadian basins of the Arctic Ocean. *Nuclear Instruments and Methods in Physics Research Section B: Beam Interactions with Materials and Atoms*, *123*(1-4), 431–437. https://doi.org/10.1016/S0168-583X(96)00677-5

Schlosser, P., Kromer, B., Östlund, G., Ekwurzel, B., Bönisch, G., Loosli, H. H., & Purtschert, R. (1994). On the 14C and 39Ar distribution in the Central Arctic Ocean: Implications for deep water formation. *Radiocarbon*, *36*(03), 327–343. https://doi.org/10.1017/S003382220001451X

Serreze, M. C., Holland, M. M., & Stroeve, J. (2007). Perspectives on the Arctic's shrinking sea-ice cover. *Science*, *315*(5818), 1533–1536. https://doi.org/10.1126/science.1139426

Slagter, H. A., Reader, H. E., Rijkenberg, M. J. A., Rutgers van der Loeff, M., Baar, H. J. W. D., & Gerringa, L. J. A. (2017). Organic Fe speciation in the Eurasian Basins of the Arctic Ocean and its relation to terrestrial DOM. *Marine Chemistry*, *197*, 11–25.

Smethie, W. M., Jr., & Swift, J. H. (2018). Distribution of CFCs and SF6 measured on the 2015 GEOTRACES and repeat hydrography cruises to the Arctic Ocean. Abstract CT14B-1278 presented at 2018 Ocean Sciences Meeting, 12–16 Feb., Portland, OR.

Smethie, W. M., Jr. (2017). CFC-11, CFC-12, CFC-113, and SF6 measured on water bottle samples during POLARSTERN cruise PS94 (ARK-XXIX/3) to the Arctic Ocean in 2015. https://doi.org/10.1594/PANGAEA.872956

Smith, J. N., Moran, S. B., & Macdonald, R. W. (2003). Shelf-basin interactions in the Arctic Ocean based on ^{210}Pb and Ra isotope tracer distributions. *Deep-Sea Research Part I: Oceanographic Research Papers*, *50*(3), 397–416. https://doi.org/10.1016/S0967-0637(02)00166-8

Soetaert, K., & Herman, P. M. J. (2008). *A practical guide to ecological modelling: Using R as a simulation platform*. Netherlands: Springer.

Spreen, G., Kwok, R., & Menemenlis, D. (2011). Trends in Arctic Sea ice drift and role of wind forcing: 1992–2009. *Geophysical Research Letters*, *38*, L19501. https://doi.org/10.1029/2011GL048970

Stedmon, C. A., Amon, R. M. W., Rinehart, A. J., & Walker, S. A. (2011). The supply and characteristics of colored dissolved organic matter (CDOM) in the Arctic Ocean: Pan Arctic trends and differences. *Marine Chemistry*, *124*(1-4), 108–118. https://doi.org/10.1016/j.marchem.2010.12.007

Trimble, S. M., Baskaran, M., & Porcelli, D. (2004). Scavenging of thorium isotopes in the Canada Basin of the Arctic Ocean. *Earth and Planetary Science Letters*, *222*(3-4), 915–932. https://doi.org/10.1016/j.epsl.2004.03.027

Ulfsbo, A., Cassar, N., Korhonen, M., van Heuven, S., Hoppema, M., Kattner, G., & Anderson, L. G. (2014). Late summer net community production in the central Arctic Ocean using multiple approaches. *Global Biogeochemical Cycles*, *28*, 1129–1148. https://doi.org/10.1002/2014GB004833

Woodgate, R. A., Aagaard, K., Muench, R. D., Gunn, J., Björk, G., Rudels, B., et al. (2001). The Arctic Ocean boundary current along the Eurasian slope and the adjacent Lomonosov ridge: Water mass properties, transports and transformations from moored instruments. *Deep Sea Research Part I: Oceanographic Research Papers*, *48*(8), 1757–1792. https://doi.org/10.1016/S0967-0637(00)00091-1